Section A-Research paper
ISSN 2063-5346

DESIGN AND ANALYSIS OF BLAST VALVE

AAQIB MUSHTAQ BHAT , M.TECH STUDENT AT RAYAT BAHRA UNIVERSITY PUNJAB , INDIA
EMAIL :bhataaqib614@gmail.com

VARINDER SINGH , ASST.PROFESSOR DEPT. OF MECHANICAL ENGINEERING AT RAYAT BAHRA UNIVERSITY PUNJAB , INDIA
DOI:10.48047/ecb/2023.12.si4.1565

With the advancements in weapon technology, ammunition has become more precise and lethal. The civil structures required for storage of ammunition and for carrying out special operations have become vulnerable to the blast and shock loads of modern weapon systems. There is a need for innovative and indigenous design of Blast Valve which can fulfil the requirements of ventilation of such structures. The design demands that this device shall be automatic, inexpensive, reliable) and Computational Fluid Dynamics (CFD) are employed for modelling and simulation of blast valve. The shock-structure interaction analysis of different configurations of the blast valve are performed using ANSYS AUTODYN in order to optimise the design. One of the most important components of the blast valve is circular plate exposed to blast loadings. To understand the effect of blast wave on circular plate and hemispherical shells, the experiments are performed using a shock tube test facility. Plates and shells of different thickness and curvature are subjected to varying blast loads, and strains at different locations are measured in order to optimise the same. The whole exercise in the present research work is carried out to address leakage problem in existing blast valves in order to achieve a design of blast valve with minimum or no leakage.

Based on the detailed simulations, the final blast valve design is obtained. The important features of the final design are: VLC-shaped air flow channel with the outer body materials SS304 and closure mechanism materials DOMEX 700 MC grade steel, overall length = 750 mm, outer diameter = 420 mm and inlet diameter = 100 mm. The con- necting rod is of 10 mm diameter and 614.58 mm long. Hemispherical shell with 96 mm radius of curvature with gradually decreasing thickness from 5 mm at center till 2.5 mm at periphery is used for front and rear closure. The valve is designed for incident pressure of 3 bar and 3.7 ms duration and peak reflected pressure of 7 bar. The air flow rate is 0.14 kg/s under 3000 Pa pressure difference between inlet and outlet.

1. Introduction

With the modernisation in armament technology, weapons are packed with more lethality and precision. The building structures required for storage of weapons, critical equipment and structures for carrying out special operations like command and control have become vulnerable to the blast and shock loads of modern armament systems. There is a need for designing, developing and validating new classes. of structures for storage of ammunition and critical equipment. Such facilities have to be protected against a wide range of threats including forced entry, Chemical/Biological/Radiological (CBR), airblast, ground shock, penetration, fragmentation, and damage to the structure and equipment due to explosive loading. New designs shall consider how different methods such as camouflage, concealment and deception, active defence, and manned response can reduce or limit the effectiveness of the threat.

The structures capable of withstanding extreme shock loads and remaining operational at the time of emergency are called hardened structures or hardened shelters [1]. Hard- ened structures are designed to withstand and remain operational during forced entry, ground shock, bomb penetration, fragment hit, CBRN (Chemical, Biological, Radiolog- ical and Nuclear) attacks and damage to the structure, equipment and human resource due to explosive blast/ shock. The ultimate aim of these structures is to protect man and equipment present inside from all possible range of threats to enable them to perform the desired operation. Hardened Structures are designed primarily for Weapons of Mass Destruction or WMD's/ nuclear weapons of medium to large size but also secondary for chemical, biological and radiological dispersion devices and conventional weapons. Al- though the design and dimensions are principally determined for nuclear weapons it can be established that a good underground nuclear bomb shelter also offers excellent pro- tection against chemical, biological and conventional weapons along with most types of WMD's. Nowadays, in addition to protection against conventional and non-conventional threats the importance of having EMP (Electro-Magnetic pulse) protection in Hardened structures have become important concern. A well designed hardened structure provides high degree of protection against the war effects or hostile surroundings by providing a hardened mechanical shield against the harmful conditions and sustaining life inside the hardened structure via temporary life supporting systems. All hardened structures either used for critical stores or special operations which are to be occupied by personnel for more than a few hours must have ventilation. In normal buildings, this is achieved by air intakes and exhaust ducts to the outside atmosphere but in case of a hardened struc- ture/building, these ducts must be equipped with some sort of device to prevent a blast wave from entering the sheltered area via the ventilation system.A prime concern of blast resistant structures is to prevent the flow of high pressure blast wave into or out of the structure. This requires openings to be completely sealed to prevent the diffusion of harmful contaminants along with high pressure blast wave. The simplest and most economical way of limiting leakage pressure into or out of a protective structure is to restrict the number and size of air intake and exhaust openings. Even after doing so, if the leakage pressure cannot be reduced to acceptable levels or if contaminants are released during an explosion, the openings must be sealed with either blast valves or other protective closure devices.

Blast valve is a mechanical/ electromechanical device used to protect the occupants and or critical instruments kept inside a shelter (fallout shelter or bunker or hardened structure) from the effects of sudden pressure rise during conventional or non-conventional explosion. Blast valves play important role in protecting man and machine held inside the structure from blast/ shock waves entering through window openings. In-fact all window openings of hardened structures are replaced with blast-valves to provide required ven- tilation along with adequate protection. A non-conventional weapon produces a sudden pressure rise (shock wave) of more than an atmosphere followed by sudden pressure drop even several kilometres from point of detonation. Entry of these shock waves inside the shelter can do substantial harm to occupants and equipments. Blast valve commonly placed in air intake/exhaust pipes remains open normally, but automatically closes the air flow passage on sensing of sudden pressure changes in either direction. Figure 1.1 shows application of blast valve in typical hardened structures.

In brief, a blast valve shall be automatic, reusable, reliable, inexpensive and mainte- nance free. Following features are required in a typical blast valve for its best performance:

- ^ Should be able to withstand multiple blast impacts for designed peak pressure and its duration while maintaining all functions after blasts.
- ^ It shall also not allow large pressure impulses to pass by the valve before complete closure to cause permanent damage or death of the occupants. Thus it shall be capable to completely close the air flow passage in a very short duration to assure approximately 100% impulse block rate.
- ^ During normal operating conditions, it shall not cause excessive obstruction to the rated air flow either before or after the passage of a blast wave thereby ensuring the high air flow efficiency with minimum pressure drop.
- ^ The device should be maintenance free so as to avoid servicing in hostile environment outside after

each operation. It must be able to automatically retrieve the normal ventilation functions (after the blast is over) with minimum maintenance.

Figure 1.1: Application of blast valve in typical hardened structures

Figure 1.2: Schematic of Blast Closure Valve [2]

1.1 Blast Wave

Explosion (a chemical or nuclear reaction) occurs at very high rate with violent release of energy and converts the explosive material into gases at very high temperature and pres- sure. The sudden release and transformation of potential energy into kinetic energy during a conventional explosion generates hot gases up to 30 MPa pressure and a temperature of about 3000–4000^{o}C. High pressure gases move at very high velocity (7000 m/s) away from the centre of explosion and create blast wave in the surrounding medium [28]. A moving shock wave with decaying strength is called blast wave. It may be noted that the acoustic wave propagates at sonic velocity in a linear manner whereas blast wave propagation is a nonlinear phenomenon with velocities greater than sonic [29]. The product gases with high pressure and temperature expand outward by generating pressure waves leading to shock wave. Due to very high velocity and very high temperature, the boundary layer effects are confined to a very narrow region and the flow of gaseous products is assumed to be inviscid. Thus the viscous forces are not considered for the explosive modelling [30].

The explosion in air at a considerable height from ground is known as free-field air blast with spherical waves. The key features of the free-field air blast wave [31], as shown in Figure 1.6, are:

- ٨ t_a is the arrival time when shock wave of the free air blast reaches at the point of interest.
- ٨ the pressure rises within microseconds from reference value (generally atmospheric pressure) to maximum value of pressure and then it starts decreasing.
- ٨ in the positive phase duration td+, the pressure falls from maximum value to the reference pressure.
- ٨ in the negative phase duration t_{d-}, the pressure drops below the reference pressure until it reaches the minimum value below reference pressure.
- ٨ the specific impulse I_S during positive phase or overpressure impulse is the integral of the overpressure curve given by equation 1.1

$$I_S = \int_{t_a}^{t_a+td+} p\,dt \qquad (1.1)$$

where p is overpressure as a function of time.

Blast loading on a structure depends on the mass of explosive in terms of TNT equiv- alent and stand-off-distance. One important scaling parameter called "Scale distance" is obtained by dividing stand-off-distance with cube root of equivalent mass of TNT. The blast scaling is done using Cranz-Hopkinson or cube-root scaling law [32]. It states that self-similar blast waves are produced at identical scaled distances when two explosive charges of similar geometry and of the same explosive, but of different sizes, are detonated in the

same atmosphere. The mathematical equations to calculate different blast param- eters are given by Goel et. al. [29] describing the available formulae for pressure-time history useful to simulate blast-structure interaction with a fare degree of accuracy.

1.2 Motivation and Objectives

It is understood that there is an inherent leakage problem associated with the self ac- tuating blast valve mechanism whereas a remote actuating mechanism may fail during a near miss explosion. There is a requirement for one sensing mechanism which shall work even in the case of near miss explosion. Further the response time of this sensing mechanism shall be just enough to close down the closure disc properly in order to avoid any leakage. The strength to weight ratio of moving components shall be maximum to provide minimum inertia and thus minimizing the response time. Since the blast wave approaching the valve is supersonic (M >1), and the closure disc starts from zero veloc- ity on impingement of blast wave with the average velocity of closure plate being much smaller as compared to the shock velocity, the blast pressure/shock leaks into the pro- tected area during the closing period of a blast valve. To overcome this problem, one can choose a remote actuated valve but it has other disadvantages such as complexity in operation and failure during near-miss explosions. In view of the above, the self-actuated blast closure valves are preferred. This can be achieved by using the blast wave itself to trigger closure device and provide the required power for closing. The detailed literature review reveals that the leakage of blast pressure, being an important problem, has not been analyzed in the open literature except a few reports published during 1950's by US Department of Defence. Thus there is a need to analyze different techniques for reducing the blast pressure leakage through a blast valve. It is also concluded from the literature review that the fluid-structure interaction analysis of complete blast valve and its closure plate/ shell has not been carried out. The dynamic response of hemispherical shells and circular plates both by experimental methods and numerical simulations has not been reported much and only static and dynamic finite element analyses of square and circular plates for various support conditions has been studied in the literature. There is a need for experimental and numerical studies of hemispherical shells and circular plates under shock loading for varying thickness, radius of curvature and loading conditions. The FSI modelling and simulation of complete valve assembly need to be performed to obtain op- timum path for flow of shock wave, structural response of moving components, stresses and failure zones of different components in order to address the challenges associated with the blast valve.

In view of the literature review findings, the main aim of the present study is to design a valve which has ideally no leakage problem. The objectives set for the study are:

1. To conceptualize the valve design with minimal blast leakage.
2. Flow and leakage analysis of conceptualized design.
3. Experimental and Numerical study of hemispherical shells/ circular plates for closure mechanism of the valve.

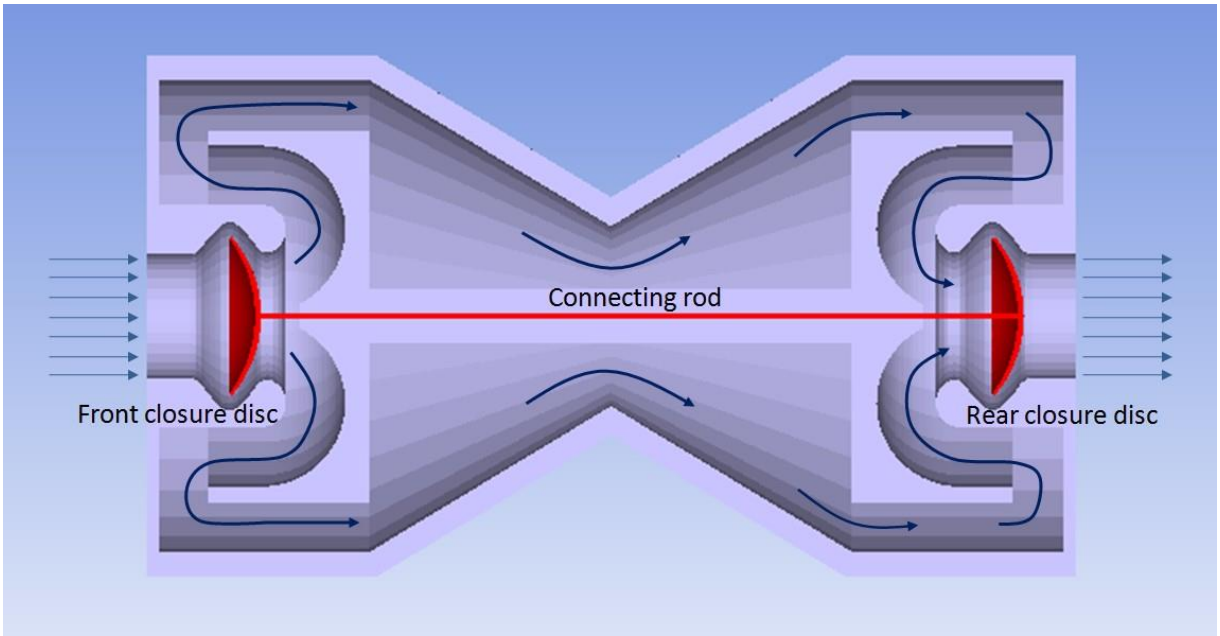

Figure 1.10: Half section of 3D Model of the one of the configurations of proposed design

4. Study of valve flow passage configuration using ANSYS AUTODYN for complete leakage prevention.

2.1 Dimensional Analysis

In the words of great researcher Bridgman [28] "The principal use of dimensional analysis is to deduce from a study of the dimensions of the variables in any physical system with certain limitations on the form of any possible relationship between those variables. The method is of great generality and mathematical simplicity". At the heart of dimensional analysis is the concept of similarity. Thus under some very particular conditions, there may be a direct relationship between the forces acting on a full-size blast-valve and those on a small-scale model of it.

Table 2.1: Parameters of Dimensional Analysis

Sr. No.	Physical Parameters	Symbol	Units	Dimensions
1.	Valve Closing Time	t_c	*Sec*	T
2.	Characteristic Length	L	m	L
3.	Modulus of Elasticity	E	Pa	$_{ML}-1_{T}-2$
4.	Overpressure	P_g	Pa	$_{ML}-1_{T}-2$
5.	Stress of Closure Plate	σ	Pa	$_{ML}-1_{T}-2$
6.	Mass Density	ρ	kg/m^3	$_{ML}-3$
7.	Initial Downstream Pressure	$Pd1$	Pa	$_{ML}-1_{T}-2$
8.	Downstream Pressure Rise	$Pd2$	Pa	$_{ML}-1_{T}-2$
9.	Poission's Ratio	v		

To simplify the dimensional analysis, few assumptions are made without departing much from the real conditions [31]. For example, frictional forces are neglected, heat transfer is also ignored due to very low interaction time, the rebound aspect is not con- sidered, the blast/shock wave is considered without any fragment hitting the valve plate. Due to these assumptions, the calculated closing time

may deviate from experimentally obtained values. Thus the theoretical dimensional analysis will give a basis for only ap- proximate design of the valve. Some important issues such as the pressure rise immediately downstream of the valve is not analyzed using dimensional analysis.

2.2 Preparation of test samples

Flat collared hemispherical shells with radius of curvature equal to 2r, 3r and 4r (where r = 50 mm, is the parallel circle radius of hemispherical portion) of for four different thicknesses 0.5 mm, 1.0 mm, 1.2 mm and 1.5 mm and flat circular plates of thicknesses
0.5 mm, 1.0 mm, 1.2 mm, 1.5 mm and 2.0 mm are chosen for the study. The driver pressure ranging from 1.5 bar to 20 bar is selected to impart shock loading on the samples till the samples are permanently deformed. The radial and hoop strains at a radial location of 35 mm are measured and compared. One more strain gauge is placed at centre of the shell in some of the samples for measuring strain at centre of the shell. The strain gauges are placed on convex side of the hemispherical shell and load is imparted on the concave side. The location of pressure transducers placed in the driven tube is 115 mm and 1065 mm from the position of sample towards the driver side. Pressure transducer Model No.PCB- 113 B21 with measuring range upto 1379 kPa is placed at 115 mm location and pressure transducer Model No.PCB-113 B27 with measuring range of 689.4 kPa is placed at other location. Further, usage of these signals from pressure transducers at two locations is helpful in deducing Mach number of the shock wave [30].

Figure 2.1: Hemispherical shell with 2r curvature and thickness 1.5 mm

Figures 2.1 and 2.2 show hemispherical shells of thickness 1.5 mm, 2r radius of curva- ture and 1.0 mm thick, 3r radius of curvature, respectively, with two biaxial strain gauges one at centre and another at r = 35 mm radius. Hemispherical shell is then loaded at the end section of driven

tube by sample holding mechanism with concave side facing the shock (Figure 2.2). The conical portion of annular ring of holding mechanism touches the hemispherical shell and forms circular line of contact between the two surfaces. The end section of driven tube is fitted with flange which is affixed with a circular rubber pad. The flat collar of hemispherical shell rests on circular rubber pad and makes leak proof surface contact when pressed by sample holding mechanism (Figure 2.3). Since the holding mechanism is a spring loaded mechanism, it allows the pressure to release after the hemispherical shell is loaded with impulse produced by shock wave.

Figure 2.4: Hemispherical shell with 3r radius of curvature and thickness 1.0 mm

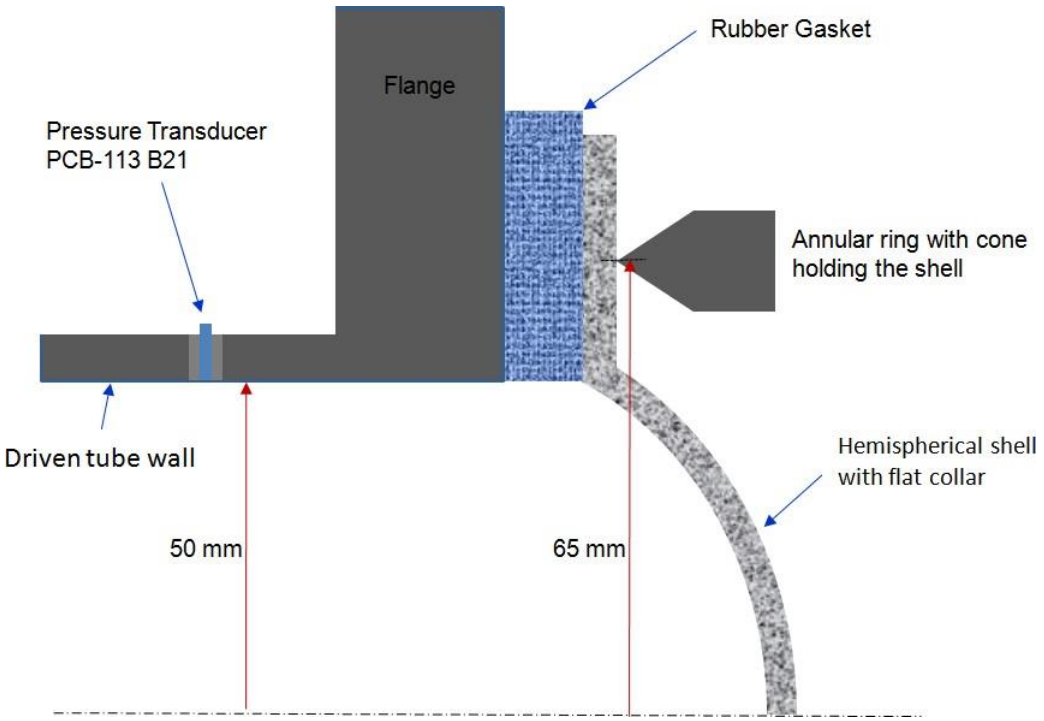

Figure 2.5 : Cross section of hemispherical shell held from both sides

2.2 Preparation for experimental evaluation

Once the sample is loaded in a predefined manner with the help of holding mechanism, the complete end portion of driven tube along with sample and holding mechanism is housed inside bullet proof polycarbonate box of size 1.0 m^3. This is required to arrest any fragment which may get generated during impulse loading of the sample. This box also serves as a chamber to settle the high pressure coming out of the shock tube. The wires of the strain gauges are taken out of this box through a small hole and connected to the Wheatstone bridge and thereafter to the dynamic strain meter. The output of dynamic strain meter is supplied to the Hioki data recorder. Similarly the output of two pressure transducers are supplied to the signal conditioner thereafter the output of

signal conditioner is supplied to the Hioki data recorder. Instrumentation is switched on and the sensors and strain gauges are tested by hand pressing and simultaneously observing the signal in Hioki data recorder. After ensuring that the instrumentation system is working properly, the quick connecting flange is opened to load the diaphragms. Based upon the operating driver pressure, the number of circular Mylar sheets (0.1 mm thick) are used to separate driver and driven section gases.

There is a diaphragm rupturing mechanism used to rupture the diaphragm when the driver is completely filled at desired pressure. The diaphragm rupturing mechanism equipped with a spring loaded sharp cone plunger is manually loaded for each operation. One knob operated electromagnetically holds the plunger under loaded condition. During operation, the knob is pulled up by electromagnetic force and plunger is released to rupture the diaphragm. As soon as the diaphragm is ruptured, the shock front moves forward to load the sample.

One of the most important aspect is the way the shock loading timing is controlled to get Friedlander profile (the ideal profile representing the blast/ shock load on a sample). As discussed at the beginning of this chapter, the duration of shock loading or in other way generation of a Friedlander profile on the sample depends on length ratio of driven to driver section for a given Mach number and given working medium. Nitrogen is used as the working medium and is filled in the driver section. The driver tube inserts are just straight cylindrical objects almost filling the driver section in diameter, with various lengths, to adjust the length of the driver section in order to get an appropriate loading profile (Friedlander profile) on the sample. For the present application, a driver tube insert of 0.53 m length is used. The tube insert is firmly attached to the driver's end flange before inserting it inside the driver from rear side and then bolts are tightened.

After placing the diaphragm and tightening the quick connect flange, the driver is required to be filled with nitrogen gas which is stored in a cylinder at about 200 bar pressure. Nitrogen cylinders are kept outside the building for safety. The 200 bar pressure of nitrogen gas is reduced through a pressure reduction valve and then supplied to driver through high pressure hose pipe. The gas received via hose pipe is released to the driver through a check valve in controlled manner. The safety guidelines are ensured before releasing pressurized nitrogen gas from cylinder and filling the driver through manually operating check valve. Once the driver is filled upto desired pressure, the check valve is closed and Hioki data recorder is triggered to record the data. The push button of diaphragm rupturing mechanism is pressed, the diaphragm is ruptured and shock wave is generated to load the sample.

3.1 Results and Discussion

For steady state flow simulation, a segregated pressure based solver is adequate with lesser computational time [99]. The governing equations are solved in segregated manner to get a converged solution. The axisymmetric and steady conditions are selected for analysis. The pressure boundary conditions are applied at both inlet and outlet with 3000 Pa and 0 Pa gauge pressure values, respectively. The problem is initially solved for first

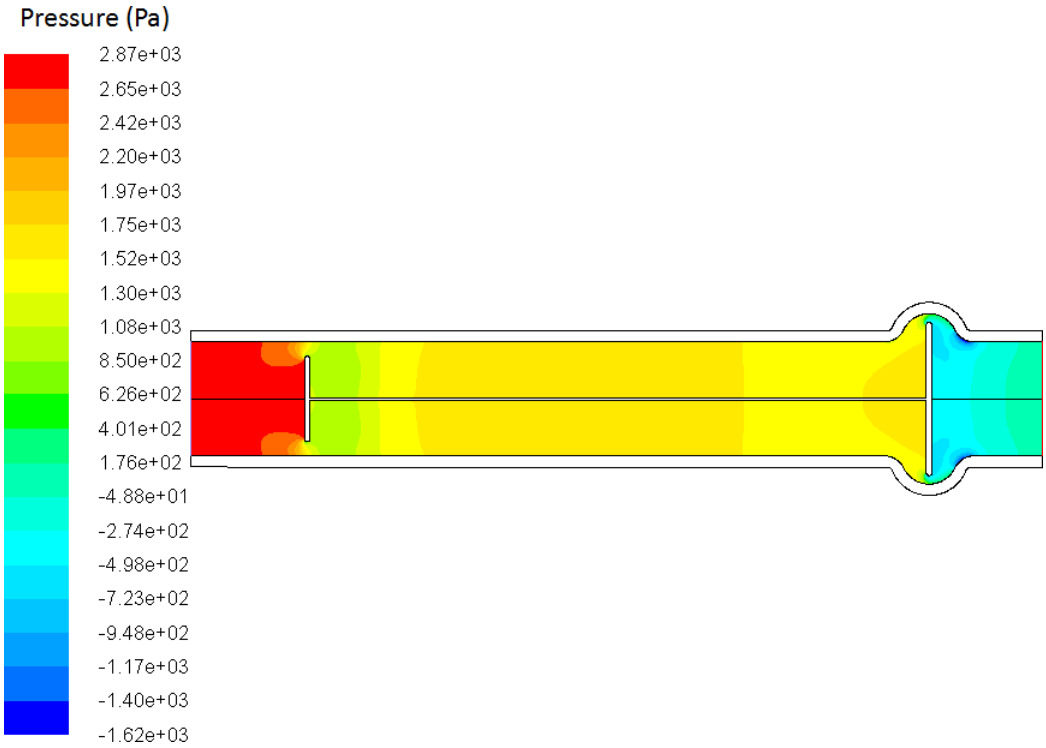

Figure 3.3: Pressur contours in the computational domain of Blast valve

order discretization for mass, momentum and turbulence equations and after obtaining the converged solution it is again solved for second order discretization to enhance the accuracy. The convergence criteria for continuity and x-momentum equations are kept as 10^{-4} and 10^{-5}, respectively. The computational fluid domain is initialized from the inlet conditions and iterations are performed.

The pressure contour, velocity contour and velocity vector plots are shown in Figures 4.3, 4.4 and 4.5. The upstream region of sensor disc shows a pressure 3000 Pa (gauge) however pressure just downstream is little negative which causes circulation as evidenced by velocity vectors shown in Figure 4.5. Upon neglecting small regions of circulation between the sensor and closure discs, the pressure upstream of closure disc is about 1500 Pa (gauge).

The zones of recirculation can be seen just downstream to sensor disc and closure disc in Figure 3.4. The blue colour contours represent the zero velocity in the computational domain. The maximum velocity in the gaps near sensor disc and closure disc is ranging

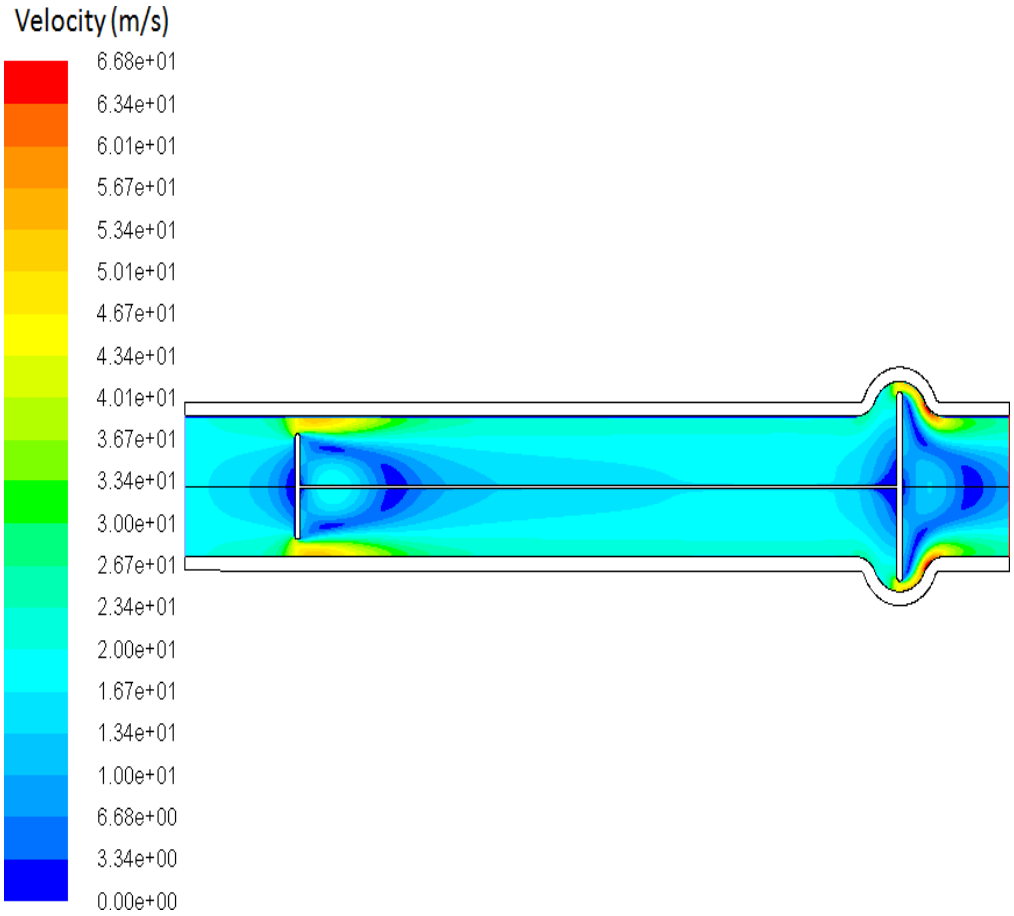

Figure 3.4: Velocity Contours in the computational domain of Blast valve

between 50-70 m/s (Figure 4.4).

The velocity vector plot clearly shows the different zones in the computational domain. Due to the obstruction, most of the fluid is moving through the annular passage with maximum velocity of about 70 m/s. The velocity vectors just downstream of sensor disc clearly show the regions of circulation. It can also be seen that the flow becomes stagnant just upstream of the sensor disc. The similar observation is made near the closure disc also.

The velocity magnitude plot along the axis of blast valve is shown in Figure 4.6. It can be clearly deduced that the flow enters the blast valve with a velocity of about 18 m/s which suddenly becomes zero at 0.1 m (just upstream of sensor disc). The velocity at the axis remains zero in the region of 0.1 m - 0.65 m due to the existence of solid domain (connecting rod) of 5 mm diameter. The velocity magnitude again starts from zero just downstream to the closure disc and reaches the maximum value of 14.0 m/s and again becomes zero due to flow recirculation.

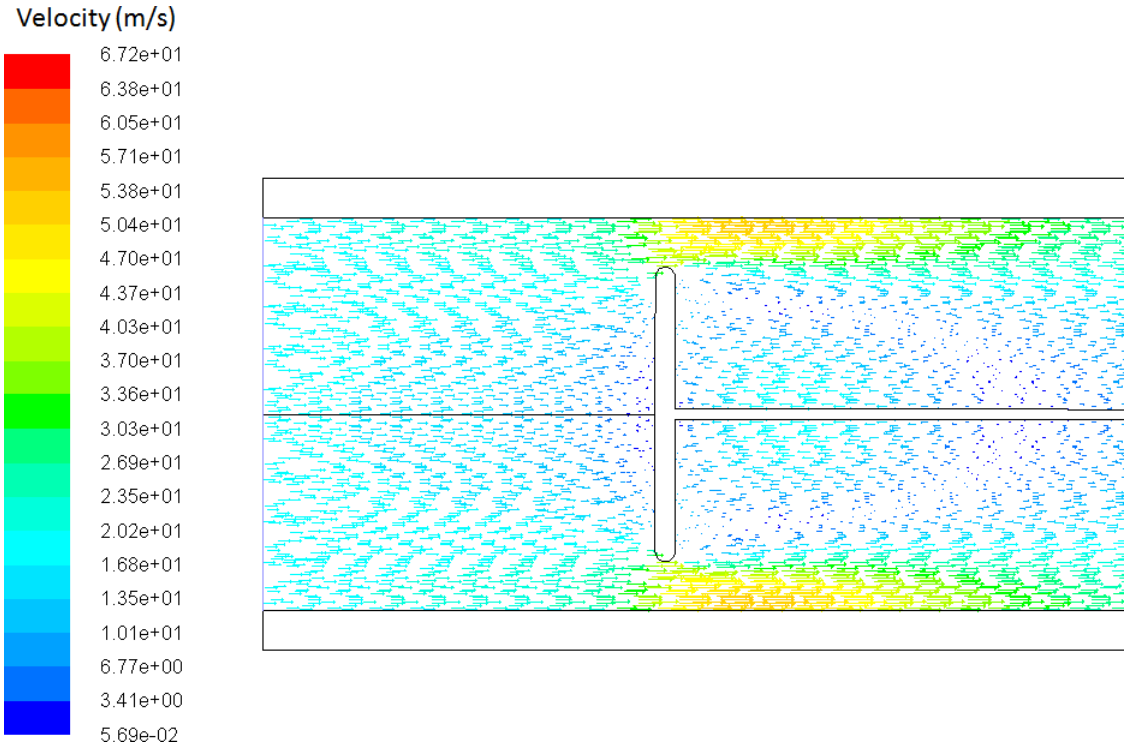

Figure 3.5: Velocity vector near inlet of Blast valve

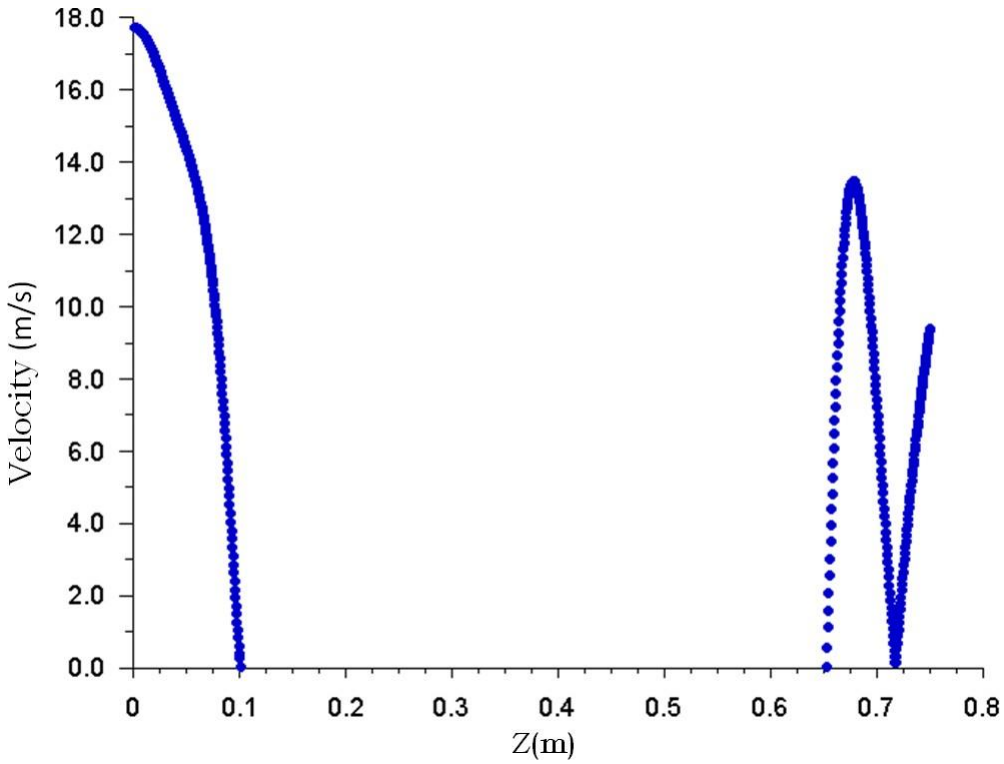

Figure 3.6: Velocity magnitude plot along the axis of Blast valve

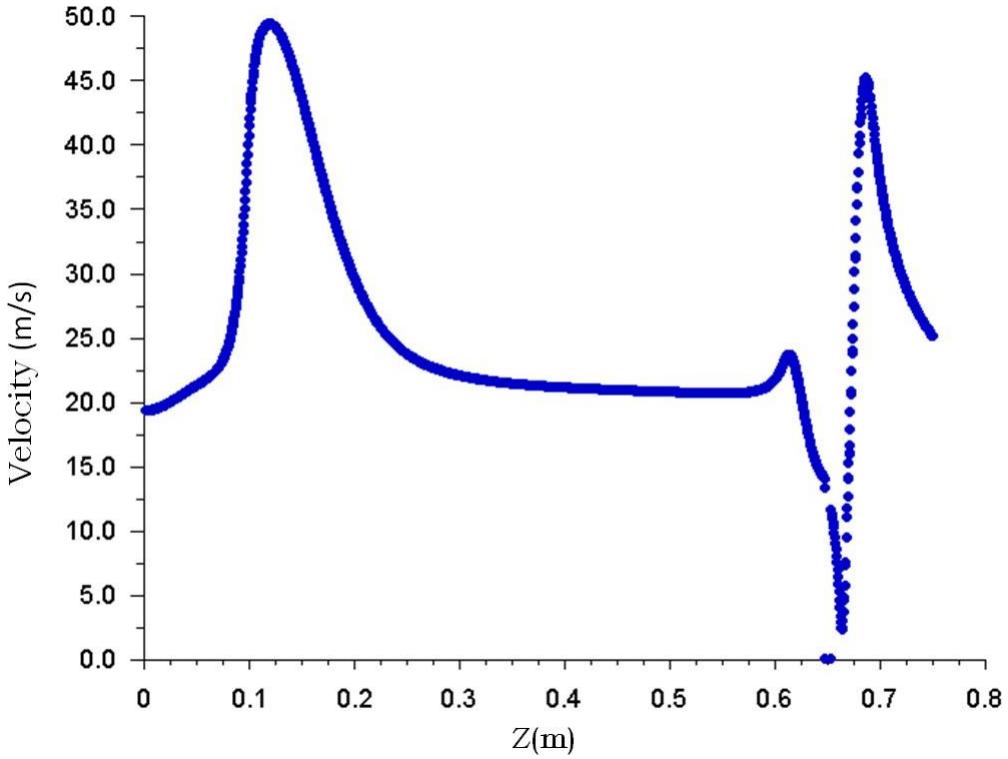

Figure 3.7: Velocity magnitude plot in annular space (at y = 0.045 m) of Blast valve

The velocity magnitude plot in the annular space at y = 0.045 m is shown in Figure 3.7. The velocity magnitude at the inlet is about 18 m/s which increases upto 50 m/s at x = 0.1 m and then decreases to 22 m/s at x = 0.6 m. The velocity then becomes zero due to stagnation at closure plate and further increases to the maximum value of 45 m/s. There is a drop in the velocity in the wider zone after the closure disc.

After analyzing the velocity vector and contour plots, it is clear that the flow of air is mostly smooth under normal operating conditions. The zones of recirculation behind the sensor disc and closure disc are unavoidable as there are regions of negative pressure gradients. The flow in the enlarged portion is almost streamlined due to its smooth entry and exit. The steady state mass flow rate obtained from simulation is 0.18 kg/s.

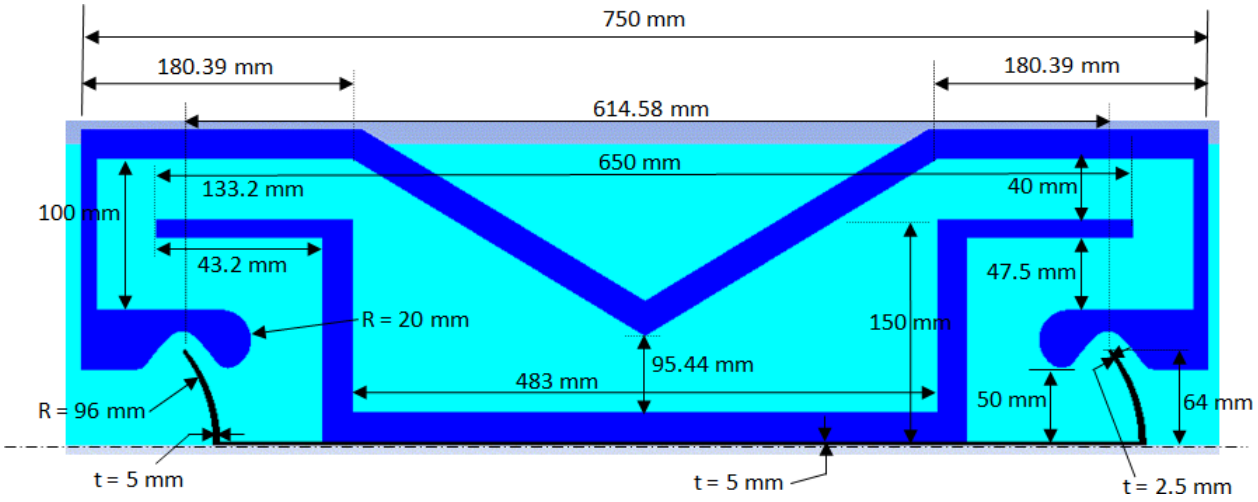

Figure 3.8: Geometric details of final design of blast valve

For steady state flow simulation, segregated pressure based solver is selected to obtain converged solutions. The air is considered as incompressible fluid and governing equations of continuity and momentum are solved in segregated manner. The pressure boundary conditions are applied at both inlet and outlet with 3000 Pa and 0 Pa gauge pressure values, respectively. The fluid flow problem is solved with second order discretization of mass and momentum. The convergence criteria for continuity and x-momentum equations are kept as 10^{-4} and 10^{-5}, respectively. The computational fluid domain is initialized with $p = 0$, $u = 0$ *and* $v = 0$ (where u, v and p are the axial velocity, radial velocity and pressure respectively) of the flow domain and iterations are performed. The results are presented in the form of contour and vector plots.

Mesh convergence study is carried out to check that the solution obtained is indepen- dent of mesh size. The fluid domain meshed with 1.25 mm and 0.5 mm quadrilateral control volumes (Figure 3.10). The two mesh sizes are chosen so that the minimum edge length of the closure shell (2.5 mm) be fitted accurately with the selected mesh. First point at the inlet, second point upstream of the front closure shell and third point down-

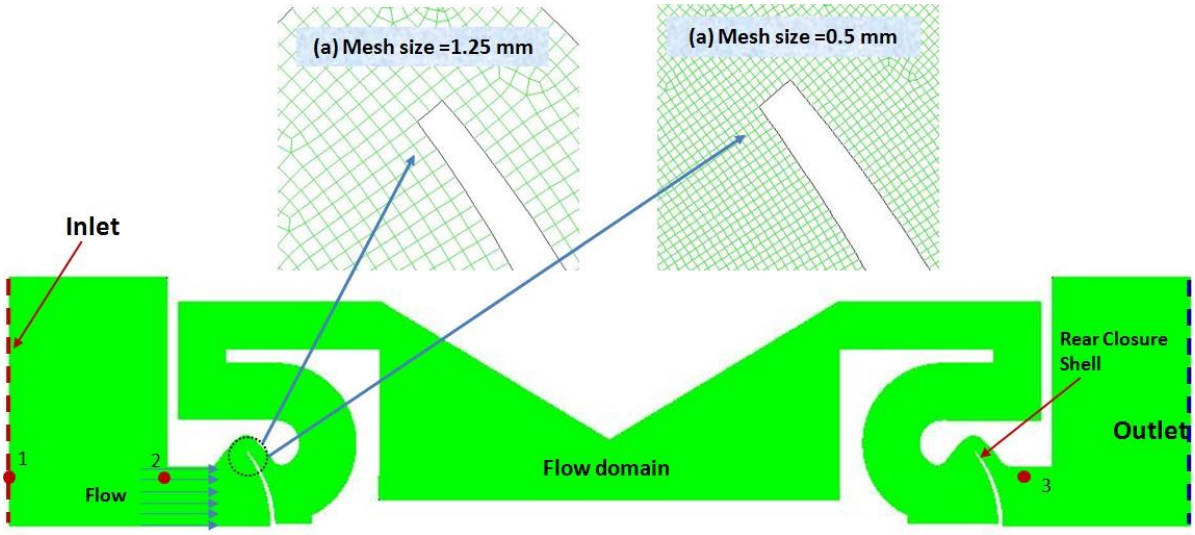

Figure 3.10: Fluid domain near front closure shell with three mesh sizes

stream of the rear closure shell (Figure 3.10, a) has been considered for comparison of results. Pressure and velocity at these two points are obtained for these two mesh sizes and results obtained are presented in Table 4.1. It is found that the variation of results between 1.25 mm mesh size and 0.5 mm mesh size is between 0.002% to 7.5%. It can be concluded from the tabulated data that the results obtained for 0.5 mm mesh size can be considered as accurate enough.

The steady state velocity vectors are shown in Figure 3.11. It can be observed from the figure that the maximum velocity is around 65 m/s in the regions of minimum air flow passage gap, i.e. the gap between hemispherical closure shell and valve body. Flow circulations are observed near the 90^o bend of V-section of flow domain. Figure 3.12 shows the pressure contours in the flow domain. The upstream of the front hemispherical closure shell shows a pressure of 3000 Pa which is developed by a blower/ axial exhaust fan capable of producing about 3000 Pa pressure difference. About 50% pressure drop is seen across the front hemispherical closure shell with formation of a zone of negative pressur near the end of C-section of the flow channel (Figure 3.12). About 10% pressure drop takes place in the CLV channel which exists between front hemispherical closure shell and rear hemispherical closure shell and rest 40% pressure drop takes place in the minimum air flow passage gap near the rear hemispherical closure shell (Figure 3.13). Figure 3.14 showing the variation of

velocity along length of blast valve depicts the region of stagnation as well as regions of sudden rise in the velocity values in the zones near the minimum air flow passage gap of both front and rear hemispherical closure shells.

Table 3.1: Comparison of results for 1.25 mm and 0.5 mm mesh size

Location	**Parameter**	**Mesh Size 1.25 mm**	**Mesh Size 0.5 mm**	**% Variation**
At inlet (x=-200 mm, y=45 mm)	Velocity (m/s)	1.583	1.547	2.27
	Pressure (Pa)	2998.46	2998.53	0.002
Upstream of front closure shell (x=-100 mm, y=45 mm)	Velocity (m/s)	5.087	5.14	1.04
	Pressure (Pa)	2984.13	2967.93	0.54
Downstream of rear closure shell (x=650 mm, y=45 mm)	Velocity (m/s)	43.32	45.52	5.07
	Pressure (Pa)	-344.99	-318.91	7.5

4.1 Concluding Remarks

The velocity vector and contour plots show that the flow of air is mostly smooth un- der normal operating conditions. The zones of circulations behind the front and rear hemispherical closure shells are insignificant due to streamlined flow due to smoother bodies near the zone of minimum air flow passage. The other zones of circulations in the C-section and in the V-section near 90^o bend are unavoidable as there are regions of negative pressure gradients. The advantage of these zones can be seen during blast when these zones will heavily contribute in attenuating the blast wave. The steady state mass flow rate obtained from the steady state simulation is 0.14 kg/s.

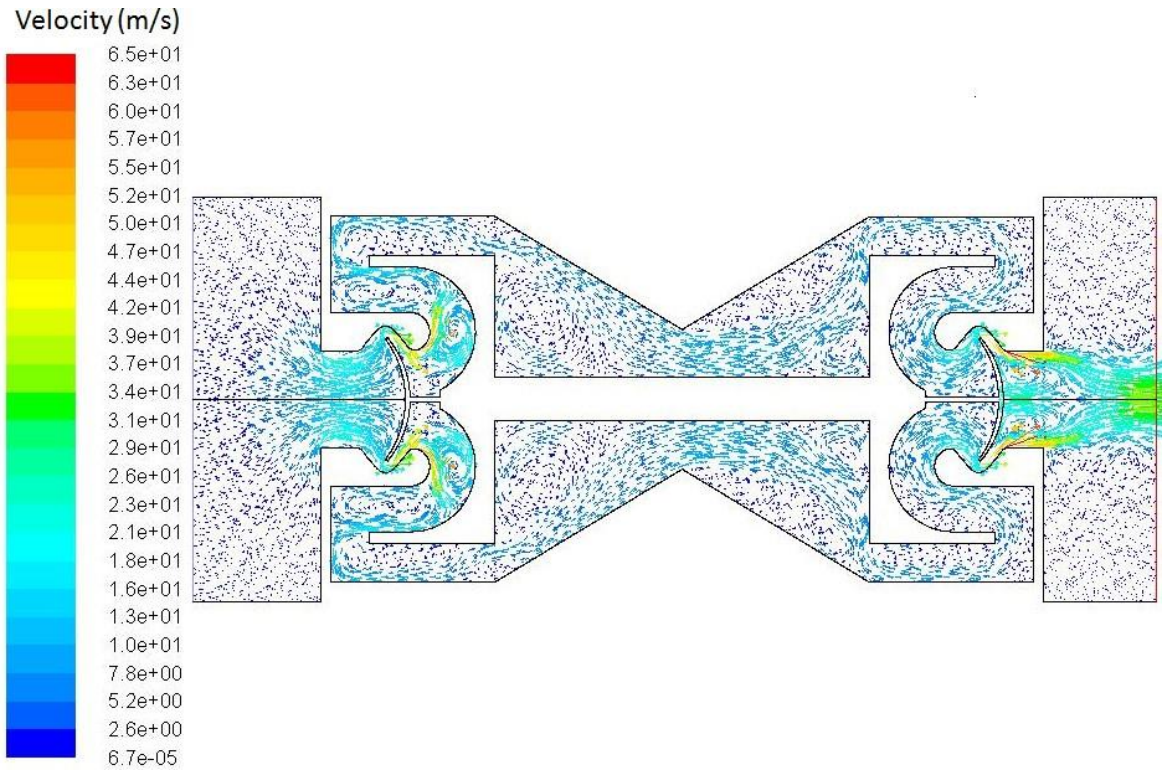

Figure 4.11: Velocity vectors coloured by velocity magnitude(m/s)

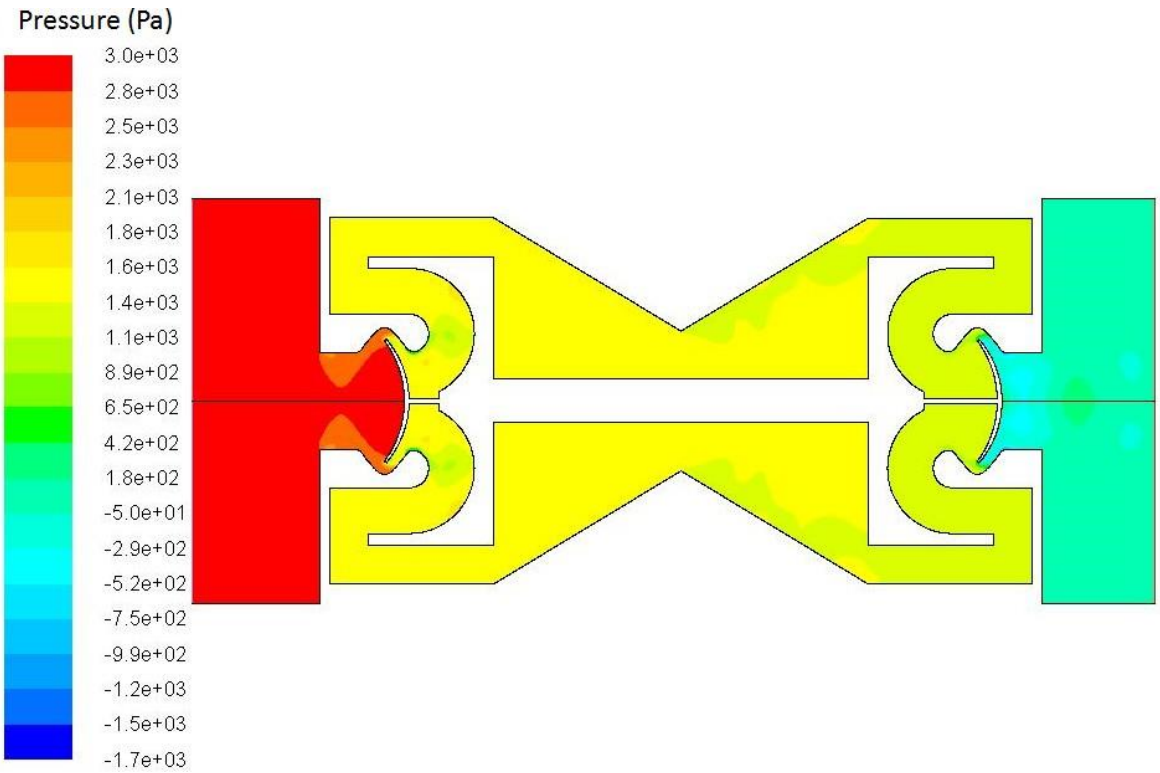

Figure 4.12: Pressure contours coloured by pressure magnitude in Pa

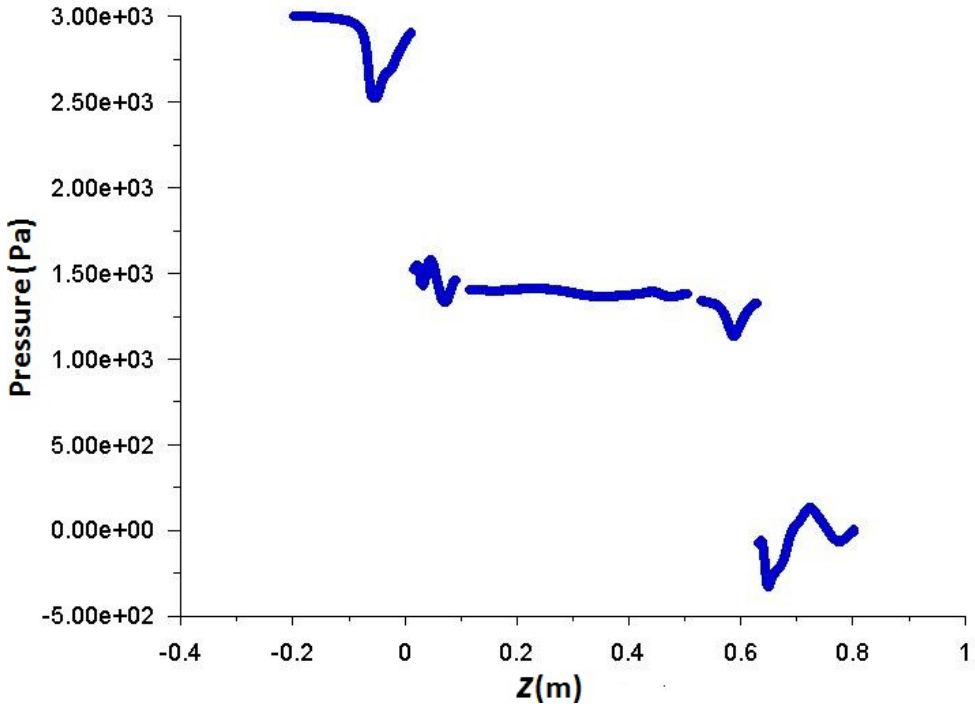

Figure 4.13: Plot of pressure magnitude along the length of blast valve at r = 45 mm

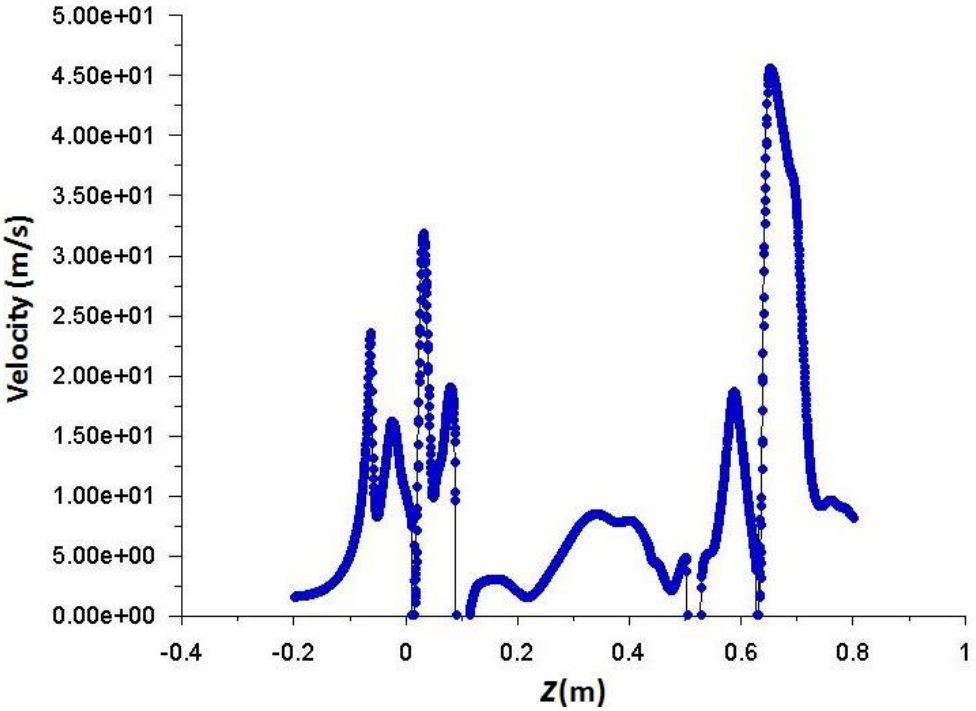

Figure 4.14: Plot of velocity magnitude along the length of blast valve at r = 45 mm

4.2 Numerical modelling/ simulation and its validation with experiments

Numerical simulation in ANSYS Autodyn is carried out to analyze shock response of samples. Axisymmetric model of test setup with hemispherical shell of 1.5 mm thickness and 150 mm radius of curvature as shown in Figure 5.8 is considered for simulation. Shock tube wall made up of SS304 is modelled as rigid material and fixed boundary condition is applied at right edge of annular support ring made up of SS304. Johnson Cook strength model (Table 3.4) and Johnson Cook failure model (Equation 3.33) for SS304 are used to model the flat collared hemispherical shell. The inner surface (concave side, r : 0 *to* 50mm) of the hemispherical shell exposed to the blast/ shock produced by shock tube is loaded with pressure time history obtained from experiments for driver pressure ranging between

7.5 bar to 20 bar. The meridional strain at (r = 0) and meridional and hoop strains at

(r = 35mm) are obtained and compared with the experimental results.

Lower driver pressure ranging between 1.5 to 5.0 bar is used to impart blast/ impact load on circular plates (thickness: 0.5 mm, 1.0 mm, 1.2 mm, 1.5 mm and 2.0 mm) as they get permanently deformed when impulse is imparted with driver pressure upto 5 bar. Figure 4.9 shows a 0.5 mm thick circular plate in deformed condition when loaded with impulse produced by 5 bar driver pressure. It can be inferred from Figure 5.9 that permanent deformation can be achieved at much lower driver pressure for circular plate with 0.5 mm thickness.

Variation of incident pressure and reflected pressure on sample is plotted with respect to driver pressure varying between 1.5 to 20 bar (Figure 4.10). It can be observed that the incident pressure on the sample is always lower than that of driver pressure however the same is not true for reflected pressure. Since the impulse imparted on the test sample is due to reflected pressure, it is important to analyze reflected pressure behaviour with respect to driver pressure. For lower driver pressure (1.5 bar and 2.5 bar), the reflected pressure produced is higher than the corresponding driver pressure. For example reflected pressure for 1.5 bar driver pressure and 2.5 bar driver pressure is 58% and 53% higher than that of driver pressure, respectively. For driver pressure ranging between 5 bar and 20 bar, the reflected pressure is lower than the corresponding driver pressure. Further, as the driver pressure increases, the corresponding increase in reflected pressure keeps on decreasing. For example, reflected pressure corresponding to 5 bar driver pressure is

4.14 bar, however only 6.34 bar reflected pressure is seen corresponding to 20 bar driver pressure. The reflected pressure to driver pressure ratio corresponding to 5 bar driver pressure is 0.83 which reduces to 0.32 for driver pressure of 20 bar. The proportional rise in reflected peak pressure is not seen with respect to increase in driver pressure due to

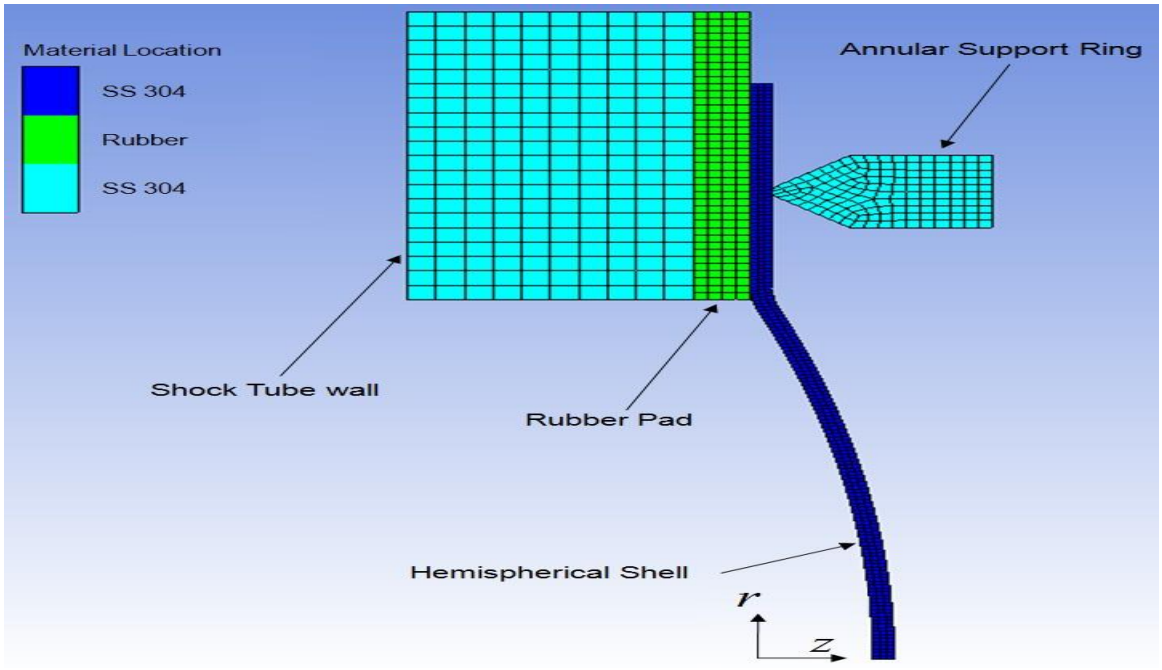

Figure 4.8: Axisymmetric model of test setup with hemispherical shell mounted

Section A-Research paper
ISSN 2063-5346

Figure 4.9: Circular plate (t = 0.5mm) deformed under impulse produced by 5 bar driver pressure

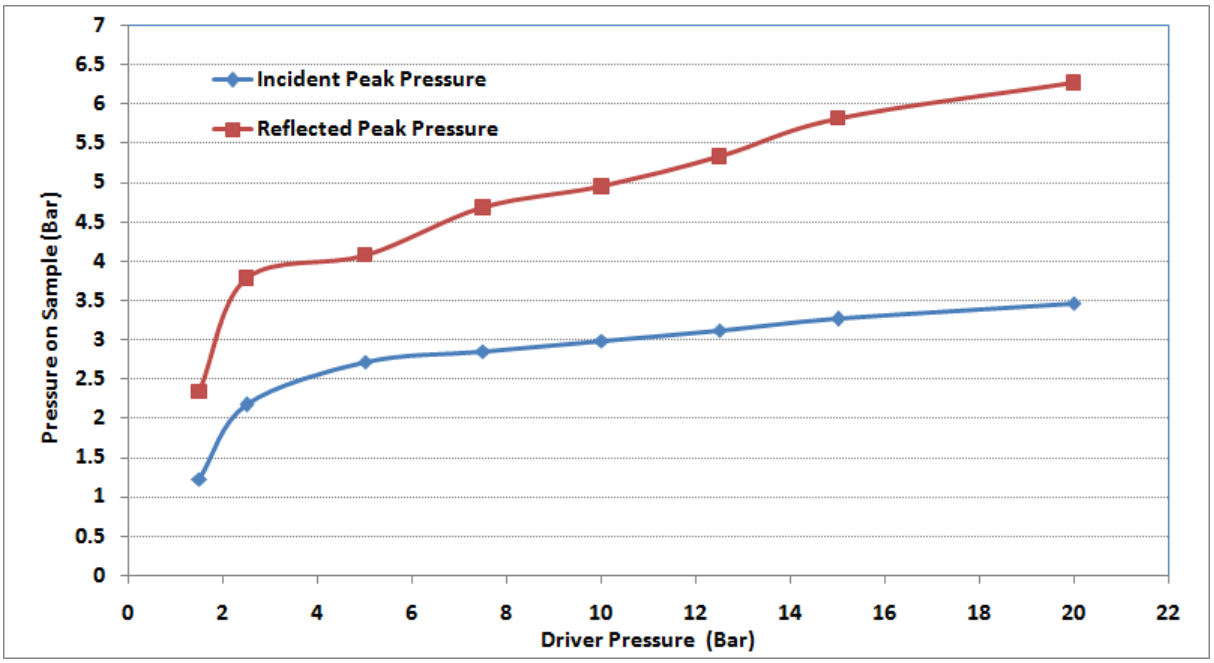

Figure 4.10: Variation of incident and reflected pressure with driver pressure

non-linear relation between reflected pressure and driver pressure resulting from adiabatic compression of gas in driven section. Similar behaviour is observed for incident pressure too. Thus, it can be concluded that that the incident/reflected pressure will not show any significant rise after certain level of driver pressure.

The output of Hioki data recorder for a typical experiment is shown in Figure 4.11 for 5 bar driver pressure. Here, horizontal axis is the time axis with a resolution of 20 ms and vertical axis is the output of strain gauges/ pressure transducers in terms of mV with a resolution of 0.01 mV. Channels 1-1 and 1-2 are showing radial strain at central location of the plate in two directions perpendicular to each other. Ideally these two plots must be identical to each other however the little difference (as observed in Figure 5.11) is due to minor misalignment from central location during pasting the strain gauge. Channels 2-1 and 2-2 show the radial and hoop strains respectively at a radial distance of 35 mm. Channel 3-1 shows the incident pressure recorded with PCB pressure transducer with 20 psi/ volt resolution and channel 3-2 shows reflected pressure with 40 psi/volt resolution. It can be seen that the reflected pressure history is a Friedlander profile which simulates the impulse imparted by blast. The incident pressure which is recorded with

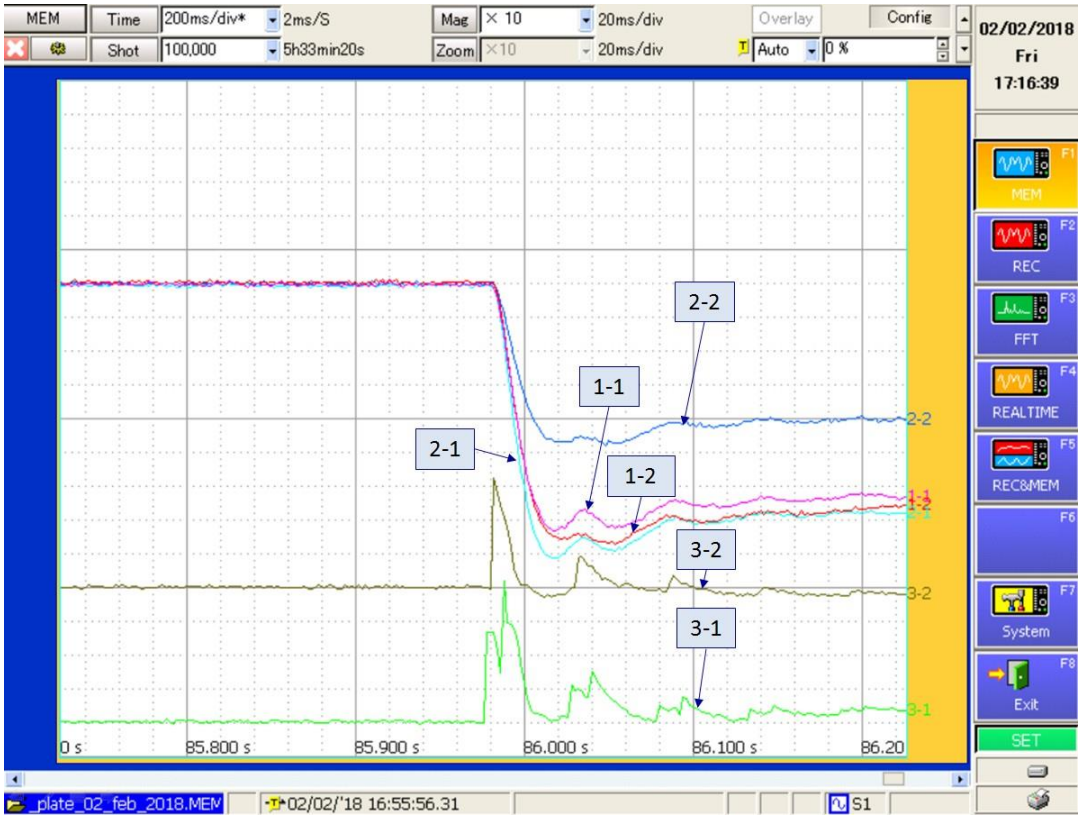

Figure 4.11: Output of Hioki-8861-50 Memory HiCorder for 1.0 mm thick circular plate

pressure transducer placed at 1065 mm ahead of the sample (towards driver) does not show the true Friedlander profile. The main advantage of using two pressure transducers is to calculate speed of shock front in addition to measurement of pressure. It can be noted that the pressure transducer placed at a location 1065 mm ahead of sample shows signal little before than that at pressure transducer placed at a location 115 mm. When the distance between these two transducers is divided with the time taken by shock front to travel between them, gives the speed of the shock front.

Simulation is carried out for a period of 5 ms and results in terms of meridional strains at $r = 0$ and at $r = 35$ *mm* along with hoop strain at $r = 35$ *mm* are obtained and plotted for 7.5 bar, 10.0 bar, 12.5 bar, 15.0 bar and 20.0 bar driver pressure and compared with experimental results obtained on shock tube for hemispherical shell of 1.5 mm thickness and 150 mm radius of curvature. The peak reflected pressure corresponding to 7.5 bar, 10 bar, 12.5 bar, 15 bar and 20 bar driver pressure are 4.68 bar, 4.95 bar, 5.33 bar, 5.82

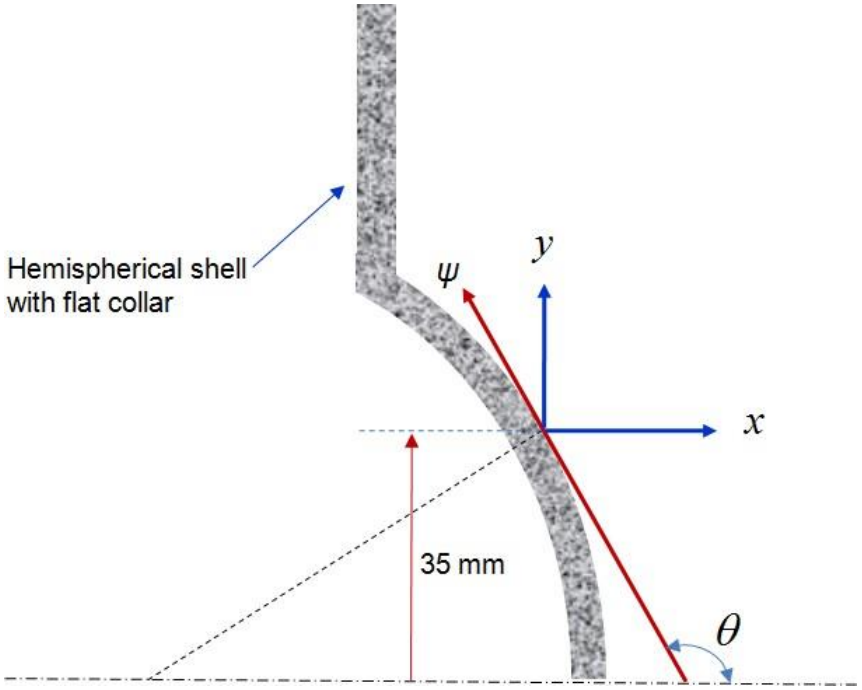

Figure 4.12: Representation of components of radial strain at r=35 mm

bar and 6.27 bar, respectively. The expression for calculating the meridional strain at $r = 35\ mm$ from the simulation results is given by:

$$\varepsilon_{\psi\psi} = \varepsilon_{xx}Cos^2\theta + \varepsilon_{yy}Sin^2\theta + \varepsilon_{xy}Sin\theta Cos\theta \quad (5.1)$$

The coordinate axis used in Equation 4.1 are represented in Figure 4.12. Here ε_{xy} is the shear strain and ε_{xx}, ε_{yy} represent the normal strains in x and y directions.

Figure 4.13 shows the plots of experimental and simulation peak strains of flat collared hemispherical shell. It can be seen that the peak meridional strain at $r = 0$ and peak hoop strain at $r = 35\ mm$ show excellent match between experimental and simulation results. Maximum deviation between experimental and simulation peak meridional strains at $r = 0$ is about 9%, minimum deviation is about 5% and average deviation is about 7%. Similarly for peak hoop strain at $r = 35\ mm$, maximum deviation is about 8%, minimum deviation is 0 and average deviation is about 4%. For peak meridional strain at $r = 35\ mm$, maximum deviation observed is about 10%, minimum deviation is about 7%

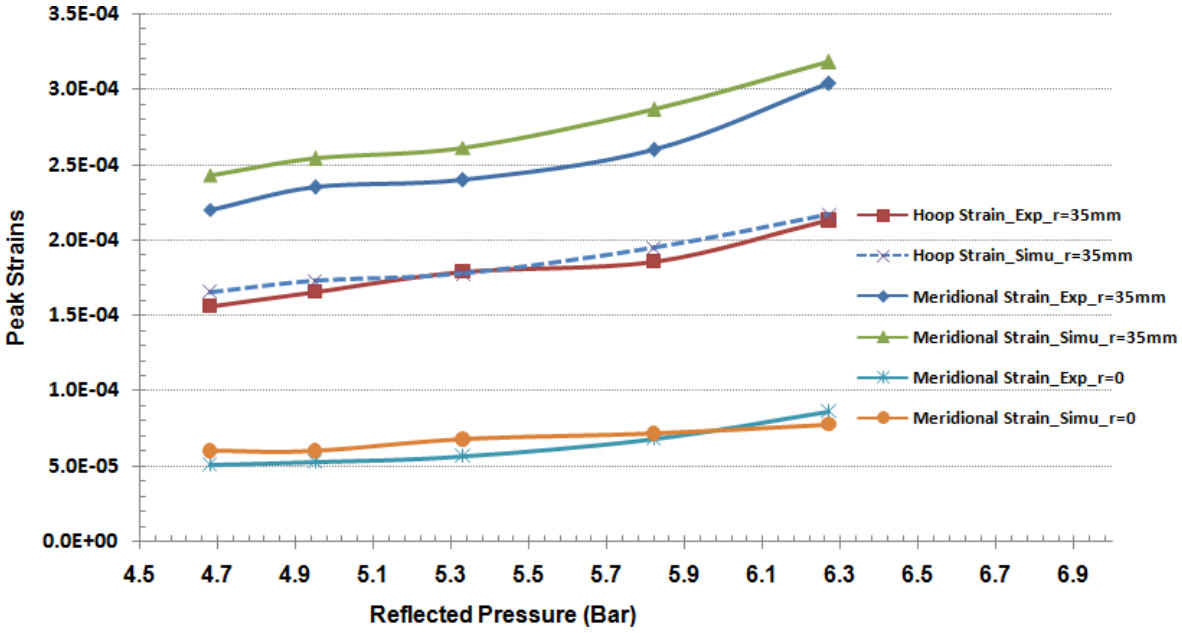

Figure 4.13: Comparison of simulation results with experimental results for 1.5 mm thick shell with 150 mm radius of curvature

with an average deviation of 9%. It can finally be concluded that the maximum deviation is not more than 10% in any of the five reflected pressures. This shows an excellent correlation between experimental and simulation peak strains.

4.2.1 Response of Circular plates: Experimental analysis

Response of circular plates of five different thicknesses 0.5 mm, 1.0 mm, 1.2 mm, 1.5 mm and 2.0 mm corresponding to impulse produced by shock tube when driver is maintained at 5bar pressure is plotted in Figure 5.14. The peak reflected pressure corresponding to 5 bar driver pressure is 4.08 bar. It can be observed that peak strains are maximum at centre and decrease with increase in radial location. Further the peak radial and hoop strains at a radial location of 35 mm plotted with plate thickness show that the magnitude of strains decrease as the thickness of plate increases. Also, it is important to note that peak radial strain is maximum at the center for flat circular plate however for hemispherical shell, peak meridional strain at $r = 0$ is minimum (Figure 4.13). Figure 5.15 shows the variation of peak strains for 2 mm thick circular plate at impulse imparted

by shock tube with reflected pressure from 2.3 to 5.3 bar. It is important to note that

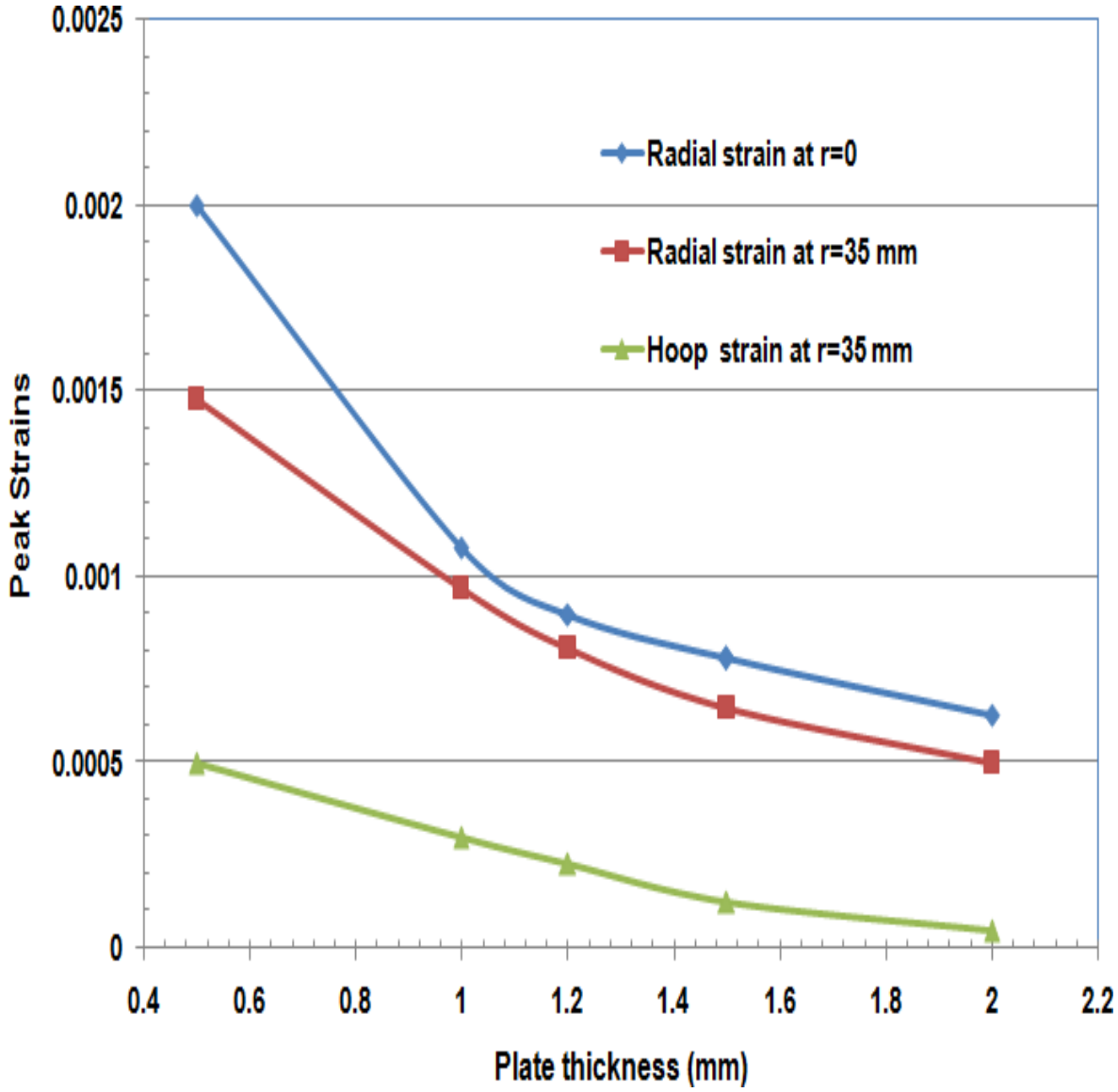

Figure 5.14: Variation of strain with thickness at 5 bar driver pressure for circular plate

the peak radial strain is maximum at center for all the pressure values ranging from 2.3 to 5.3 bar. Further, with an increase in reflected pressure, the increase in peak radial and peak hoop strains is high upto about 3 bar reflected pressure and thereafter the increase is less. Further, the increase in radial strain at r = 35 *mm* is greater than that of radial strain at r = 0 for reflected pressure upto 3 bar.

5.4 Response of flat collared hemispherical shells

5.4.1 Comparison of strain in response to impulse produced by 5 bar driver pressure

In this section, flat collared hemispherical shells of 0.5 *mm*, 1.0 *mm*, 1.2 *mm* and 1.5 *mm* thickness with three different radius of curvature ($R = 2r = 100$ *mm*, $R = 3r = 150$ *mm* & $R = 4r = 200$ *mm*) are considered. Since 0.5 mm thick shells are getting plastically deformed

Section A-Research paper
ISSN 2063-5346

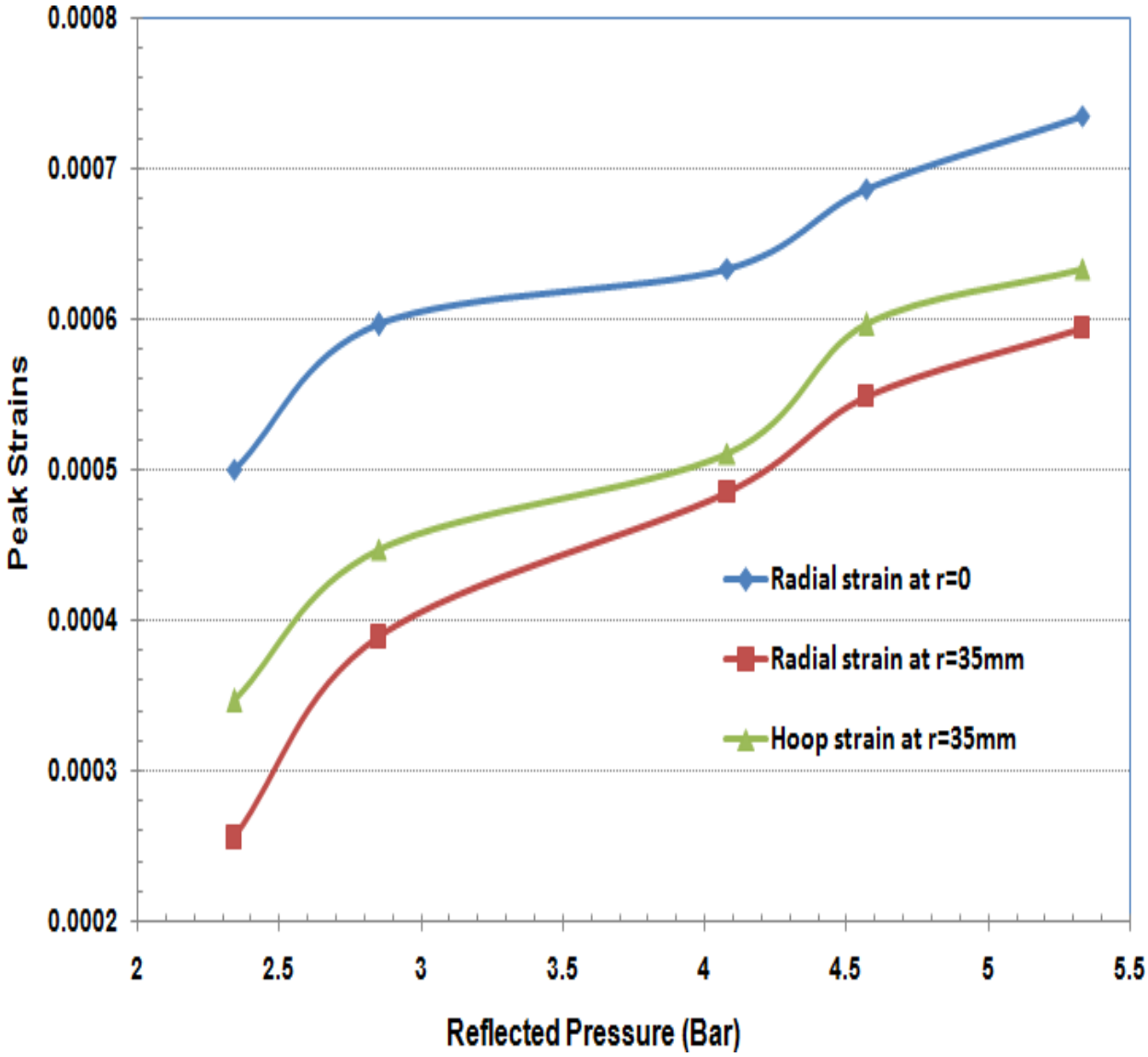

Figure 5.15: Variation of strain with reflected pressure for 2 mm thick circular plate

at lower pressures, only impulse corresponding to 5 bar driver pressure is considered. The corresponding reflected pressure is 4.14 bar. Here, peak meridional strains at $r = 0$ and $r = 35$ *mm* along with peak hoop strain at $r = 35$ *mm* are measured in response to impulse imparted by shock tube at a 5 bar driver pressure and results are plotted with shell thickness. Variation of peak strains with shell thickness at two radial locations cor- responding to impulse imparted by 5 bar driver pressure is shown in Figure 5.16. It can be observed from the figure that the strains decrease as the thickness of shell increases, which is expected. However it is important to note that the maximum strain has shifted towards periphery as the geometry changes from flat circular plate to flat collared hemi- spherical shell i.e. ($R : \infty \rightarrow 100$ *mm*) (Figure 5.14). The peak meridional strain at center is minimum.

Figure 5.17 shows photographs of 0.5 mm thick flat collared hemispherical shells with 100 mm and 150 mm radius of curvature in plastically deformed shape when loaded with the impulse produced by 5 bar driver pressure. Figure 5.9 and Figure 5.17 can be

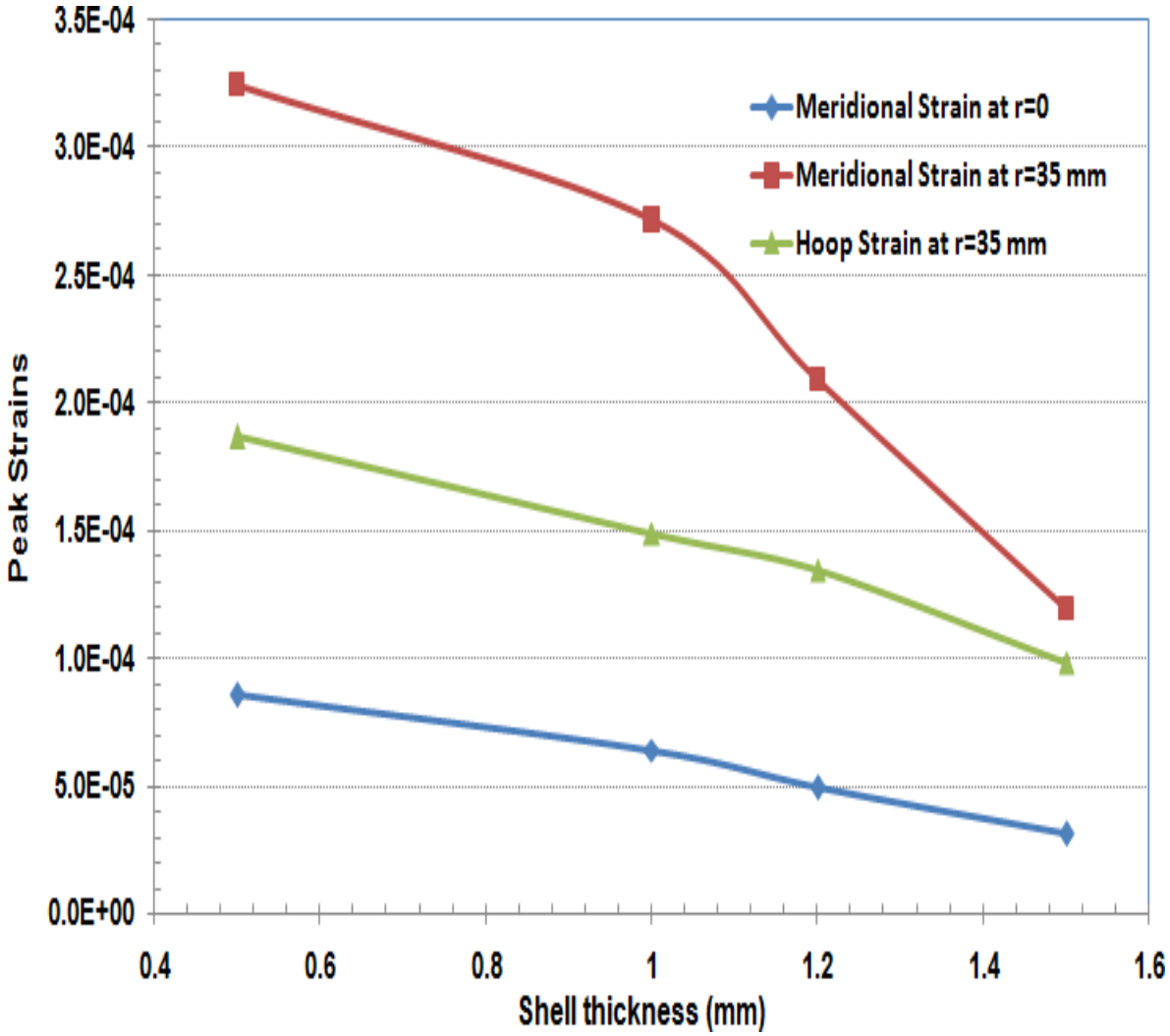

Figure 5.16: Response of shells (R = 100mm) with thickness at 5bar driver pressure

compared to see the performance of hemispherical shell in comparison to flat circular plate of same thickness. As already discussed, the plates/ shells are supported by an annular ring at at radial location of 65 mm with the help of sample holding mechanism while conducting experiments on shock tube. Figure 5.9 shows that the deformation of circular plate has propagated till center causing maximum strain at r = 0 however in case of hemispherical shells (0.5 mm thick), the deformation is seen only in annular region (r : 50 → 65 mm) where shell geometry is flat (Figure 5.17). On visual inspection it is seen that the deformation has not propagated till center in case of hemispherical shells.

Figures 5.18 and 5.19 show the response of flat collared hemispherical shells of different thickness with 150 mm and 200 mm radius of curvature, respectively. It can be seen from the figures that the peak strains decrease as the thickness of the shell increases at a fixed impulse produced by a given driver pressure. It can be noted from Figures 5.16, 5.18 and
5.19 that for a given thickness the peak strains (at both the locations) increase as the radius of curvature increases (i.e. shell becomes flatter). For example, for hemispherical shell with 0.5 mm thickness, the meridional strain at r = 35 mm is 3.25×10^{-4}, 5.43×10^{-4}

Figure 5.17: Photographs of plastically deformed 0.5 mm thick hemispherical shells

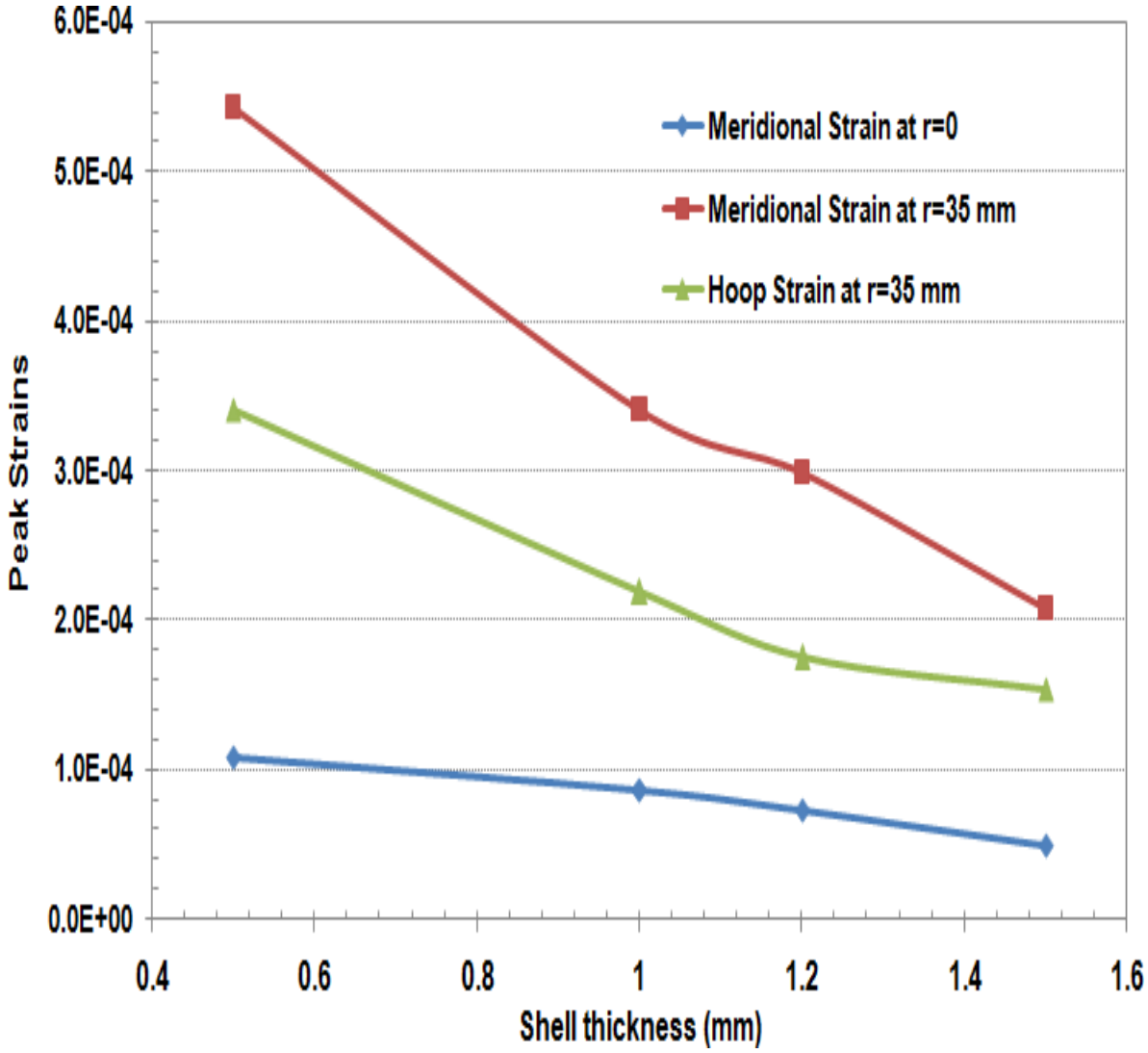

Figure 5.18: Response of shells (R = 150 *mm*) with thickness at 5 bar driver pressure

and 2.06 × 10^{-3} for R = 100 *mm*, R = 150 *mm* and R = 200 *mm* radius of curvature, respectively.

5.4.2 Response of 1 mm thick shell of three different curvatures

The deformed shape of 1 mm thick shell with 150 mm radius of curvature is shown in Figure 5.20. It can be inferred from the figure that there is no significant plastic deformation.

Figure 5.21 shows the variation of meridional and hoop strains with driver pressure ranging between 5 bar to 12.5 bar for 1 mm thick shell with 150 mm radius of curvature (Figure 5.20). Meridional strain at r = 35 *mm* is greater than the meridional strain at r = 0 with hoop strain (at r = 35 *mm*) between the two for all the pressure values. The strains increase with increase in driver pressure however for pressure between 7.5 bar and 10 bar, the rate of increase of meridional strain at r = 35 *mm* is lower. Figure 5.22 shows the comparison of strain values for all three radius of curvatures in response to impulse produced by driver pressure of 7.5 bar. It is important to note that the percentage increase

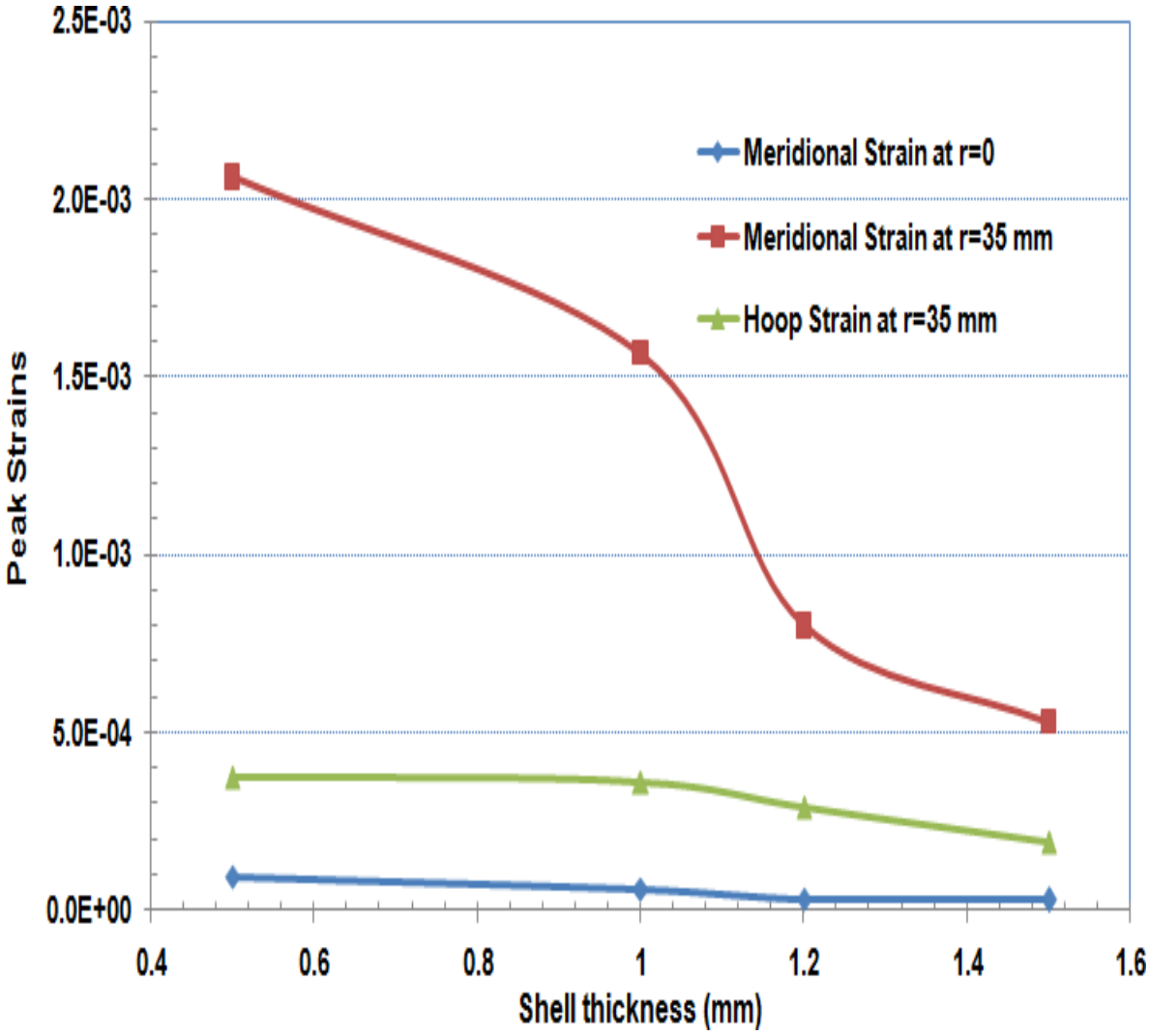

Figure 5.19: Response of shells (R = 200 mm) with thickness at 5 bar driver pressure

in strain values when radius of curvature changes from 100 mm to 150 mm is much smaller as compared to the percentage increase when radius of curvature changes from 150 mm to 200 mm especially in case of meridional strain at r = 35 mm. It can be concluded that the shell becomes stronger when the radius of curvature of the shell decreases i.e. the weight of the shell increases.

5.4.3 Response of 1.2 mm thick shell of three different curvatures

Variation of meridional strain at r = 0 against impulse produced by driver pressure ranging between 5 bar to 15 bar for flat collared hemispherical shell of 1.2 mm thickness is shown in Figure 5.23. It can be seen that the rate of increase of meridional strain at r = 0 with respect to driver pressure is maximum for hemispherical shell with R=200 mm. The shell with R=150 mm shows higher rate of increase upto 10 bar driver pressure. Hemispherical shell with 100 mm radius of curvature shows a lower rate of increase of meridional strain at r = 0 compared to other two cases. The rate of rise of meridional strain beyond 10 bar driver pressure is almost the same for shells with 100 mm and 150

Figure 5.20: 1 mm thick shell with 150 mm radius of curvature

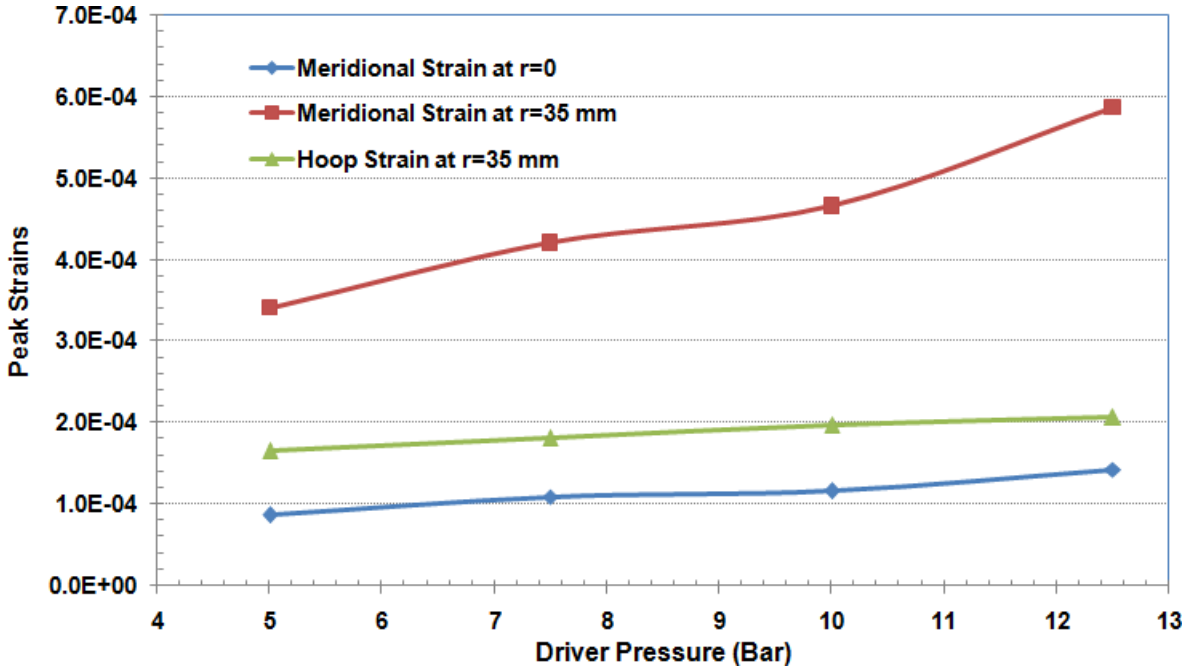

Figure 5.21: Response of 1 mm thick shell with 150 mm radius of curvature against shock loading

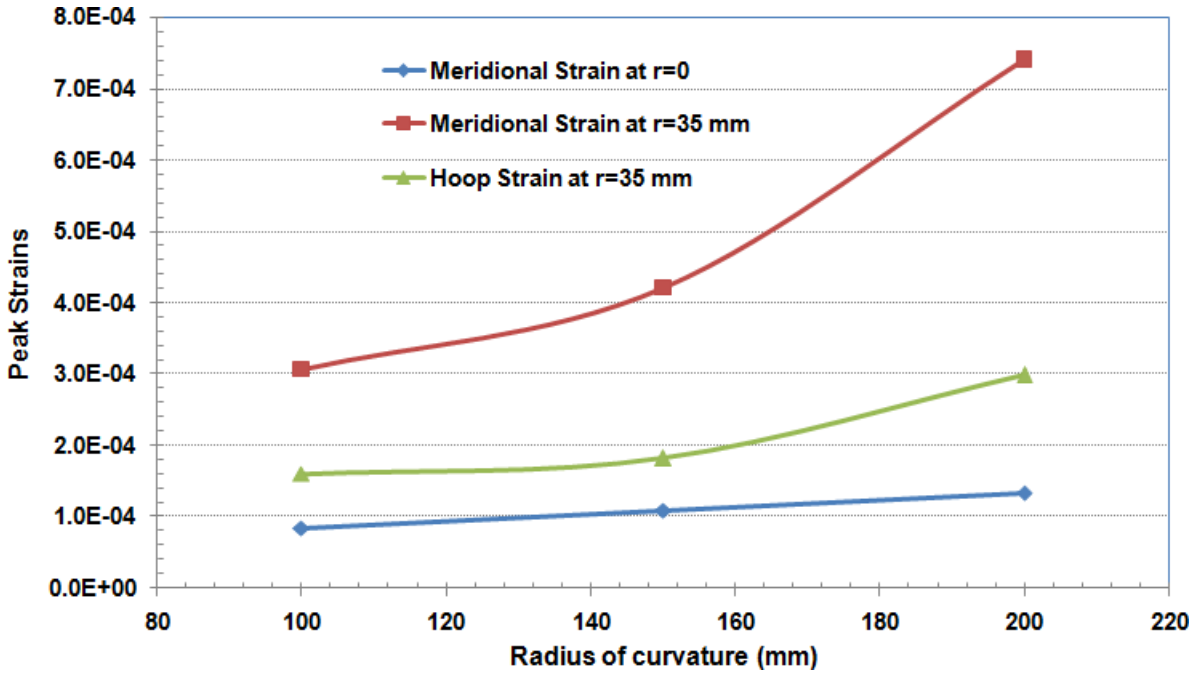

Figure 5.22: Variation of peak strains with curvature at 7.5 bar driver pressure for 1 mm thick shell

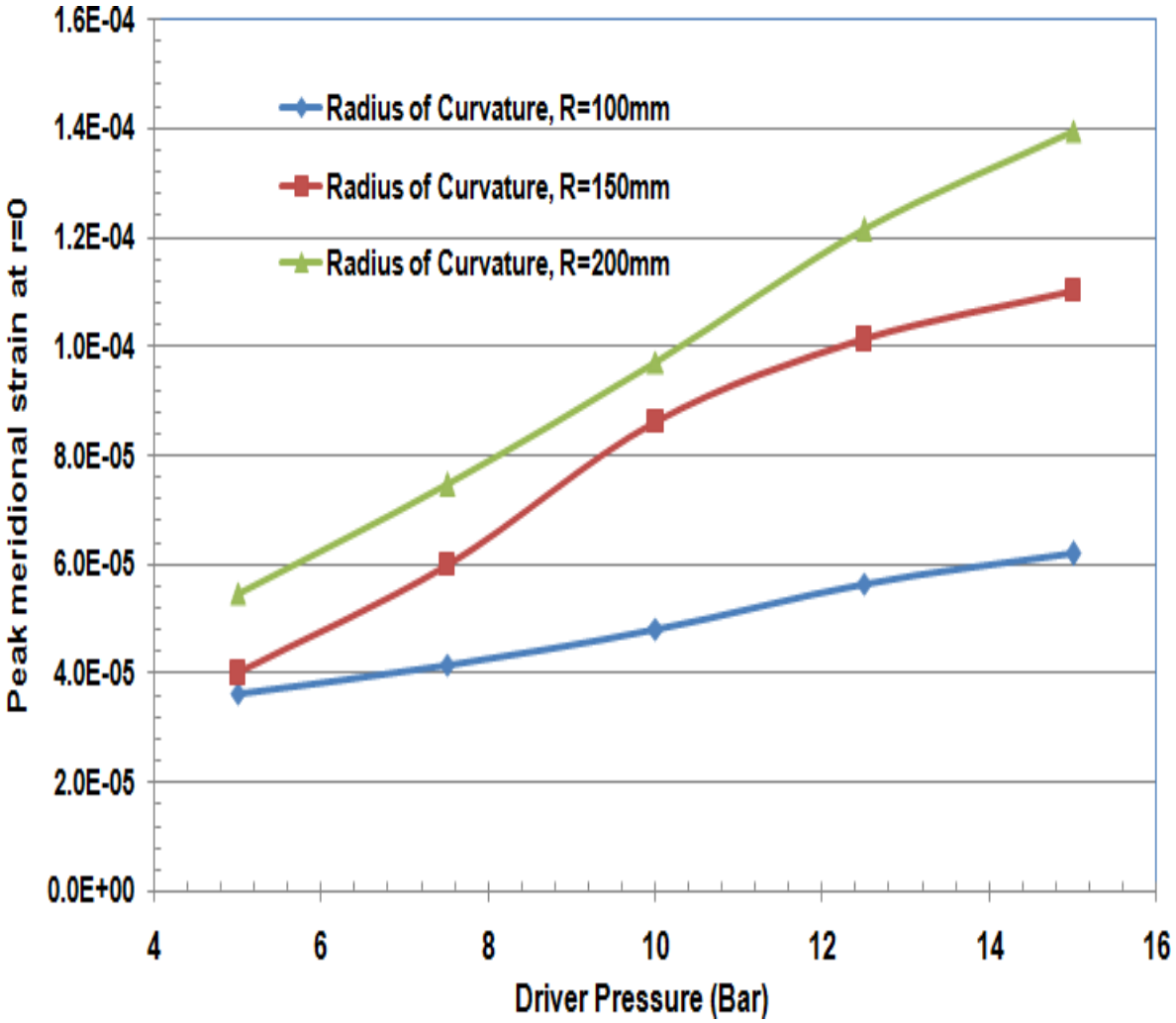

Figure 5.23: Variation of meridional strain at center with driver pressure for hemispherical shell with 1.2 mm thickness

mm radius of curvature.

Figure 5.24 shows variation of meridional strain at r = 35 *mm* corresponding to im- pulse imparted by shock tube operating with driver pressure ranging from 5 bar to 15 bar. It can be seen from Figure 5.24 that the meridional strain at r = 35 *mm* is signifi- cantly greater than that at r = 0 for all values of driver pressure and for shells with all three radius of curvatures. The important observation is that the meridional strain for shell with 200 mm radius of curvature is almost five times than that for shells with 150 mm and 100 mm radius of curvature. The increase in meridional strain at r = 35 *mm* is significantly greater when shell curvature changes from 150 mm to 200 mm. Shells with 100 mm and 150 mm radius of curvature depict almost comparable strains.

Figure 5.25 shows variation of hoop strain at a radial location of 35 mm with respect to driver pressure. It can be seen that the hoop strain at r = 35 *mm* decreases with increase in radius of curvature for a given driver pressure. This trend is opposite to the variation of meridional strain (Figures 5.23 and 5.24) where meridional strain increases with increase in radius of curvature for a given pressure.

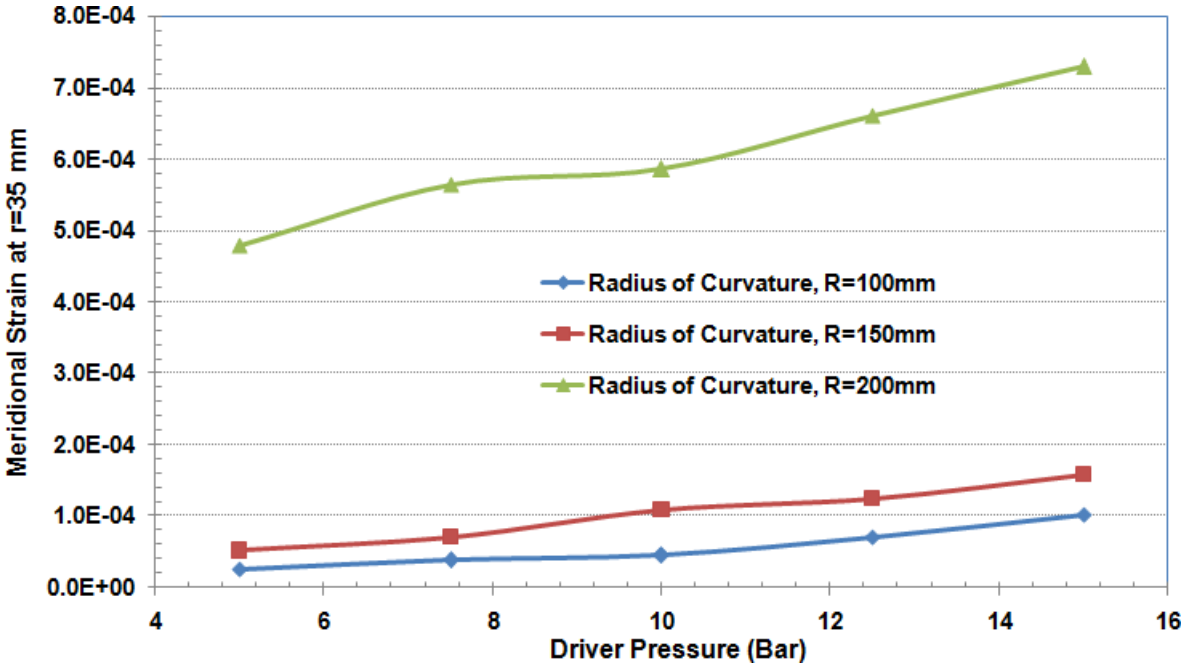

Figure 5.24: Variation of radial strain at r = 35 *mm* with driver pressure for hemispherical shell with 1.2 mm thickness

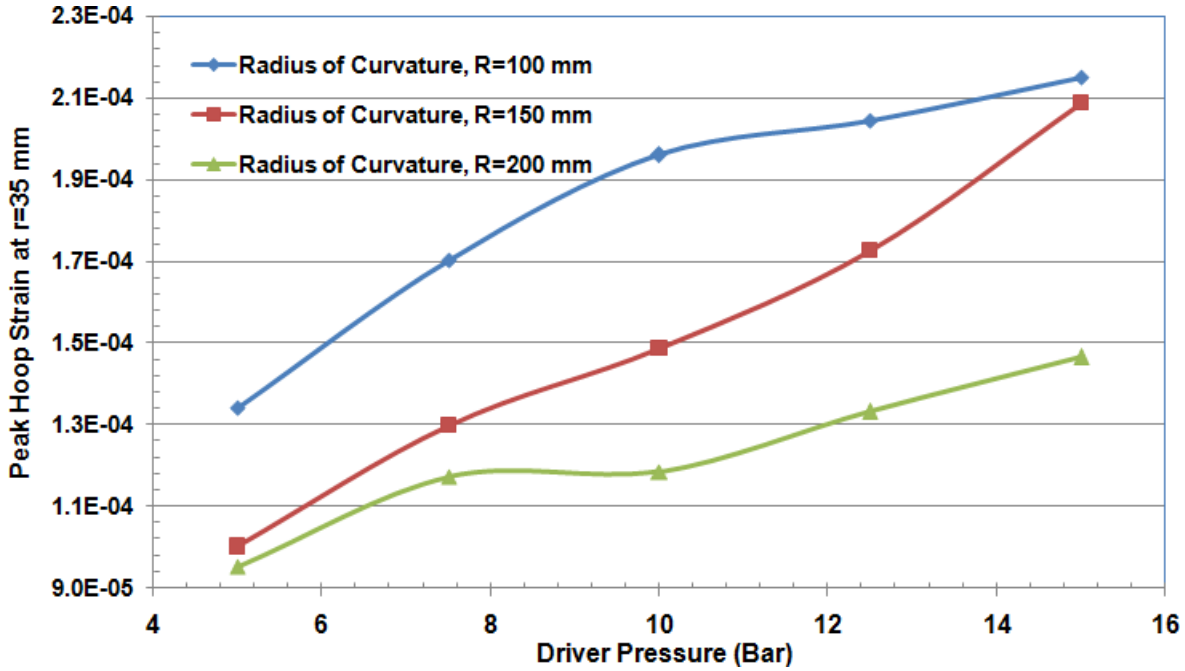

Figure 5.25: Variation of hoop strain at r = 35 *mm* with driver pressure for hemispherical shell with 1.2 mm thickness

5.5 Conclusions

Based on the detailed study, following conclusions can be drawn:

1. Simulation results obtained with ANSYS Autodyn show good agreement with experimental results for meridional strain at $r = 0$ and $r = 35$ *mm* along with hoop strain at $r = 35$ *mm* for hemispherical shell of 1.5 mm thickness and 150 mm radius of curvature.

2. For flat circular plate, radial strain is maximum at center and hoop strain is greater than radial strain at $r = 35$ *mm*.

3. For flat collared hemispherical shell, maximum value of meridional strain has shifted from $r = 0$ to $r = 35$ *mm* compared to flat circular plate.

4. With an increase in radius of curvature of hemispherical shell, the difference between meridional strains at $r = 0$ and $r = 35$ *mm* increases.

5. For hemispherical shells, meridional strain at $r = 35$ *mm* is always greater than the meridional strain at $r = 0$ with hoop strain (at $r = 35$ *mm*) between the two. Further, the variation of meridional strain at $r = 35$ *mm* shows maximum percentage increase with increase in radius of curvature followed by percentage increase in hoop strain at $r = 35$ *mm* followed by percentage increase in meridional strain at $r = 0$.

Conclusions and Scope of Future work

The research work presented here started with the aim to design a self acting blast valve to reduce the shock pressure leakage below acceptable limit. A detailed literature survey revealed that very less work on design and analysis of blast valves and its components has been reported in open literature. Having gone through the problems of existing valves (based upon literature survey), it was decided to conceptualize design of a self acting blast valve having best features of remotely acting valve. Firstly the basic calculations of closure plate and connecting rod for a reflected pressure of 7 bar are carried out to arrive at initial dimensions of closure mechanism. Next, flat collared hemispherical shells of different thickness, radius of curvature and support conditions are analyzed using ANSYS Autodyn. Based on the comparison of results of flat circular plates and hemispherical shells, it is found that the simply supported hemispherical shell loaded from concave side is suitable for closure shell. Starting with the initial dimensions, detailed shock- structure interaction analysis of different blast valve configurations is carried out. The broad conclusions drawn from the study are discussed next.

5.1 Conclusions

Based on the analysis of 09 cases of basic design of blast valve with cylindrical duct and 32 mm air flow passage gap having three configurations (double flat collared hemispherical closure shells connected with a 5 mm diameter rod, double hemispherical closure shells without any connecting rod and a single hemispherical closure shell), it is concluded that hemispherical shell of 1.5r radius of curvature is suitable for reducing the blast pressure leakage. However, high stresses developed near the region where flat collar joins the curved section of hemispherical shell and 32 mm air flow passage gap is unable to reduce the blast pressure leakage to acceptable limits.

Further, three configurations (double hemispherical closure shells connected with a rod, double hemispherical closure shells without any connecting rod and a single hemi- spherical closure shell) with reduced air flow passage gap of 14 mm and hemispherical shell (without flat collar) of 1.5r radius of curvature are analyzed using ANSYS Autodyn and it is concluded that only double shell connected with rod configuration is suitable to reduce the blast leakage. This configuration also lead to the blast pressure leakage more than the acceptable limits.

Then a C-type channel with double hemispherical closure shell connected with rod having 14 mm and 10 mm air flow passage gaps is analyzed and it is concluded that the C-type configuration with 10 mm air flow passage gap is able to stop the leakage. However, valve design with 14 mm air flow passage gap results in lower value of reflected pressure on the front closure shell.

Further 06 configurations with different air flow duct designs (LC, Modified LC, Zig- Zag, Stepper, Stepper Zig-Zag, Convergent-divergent type channels) and 15 mm air flow passage gap are analyzed with hemispherical shell having uniform thickness. It was found that all 06 designs are able to stop the leakage with 15 mm air flow passage gap, however the joint of the hemispherical shell and connecting rod is experiencing stresses beyond initial yield point of shell material (SS304).

Subsequently 03 configurations including final design (VLC-shaped air flow channel) are analyzed with hemispherical shell of non-uniform thickness(5 mm thickness at center and gradually decreasing thickness upto 2.5 mm at periphery). Based on the analysis, it is concluded that the region of higher stress is shifted to connecting rod. Two modifications

viz. cone deflector on concave side of shell and strengthening of joint on convex side are incorporated separately. However, the regions of stresses beyond initial yield point could not be removed. The connecting rod diameter is then increased to 7 mm and 10 mm and it is concluded that even a connecting rod of 10 mm diameter made up of SS304 depicts regions of von-Mises stresses greater than initial yield stress of SS304. Finally, DOMEX700MC, a special steel with 750 MPa initial yield strength, is selected and analysis with 7 mm and 10 mm connecting rod diameters is carried out. It is concluded that the blast valve design with 7 mm connecting rod diameter depicts stresses below the initial yield stress of the material, however the connecting rod of 10 mm diameter made up of DOMEX700MC is recommended for the final design. It is concluded that the final design is able to prevent the leakage completely with stress values below initial yield stress of the material for all components.

CFD analysis of final design of blast valve carried out using ANSYS Fluent depicted that the flow parameters are within the acceptable limit with air mass flow rate of 0.14 kg/s.

Shock tube tests on circular plates of different thicknesses and flat collared hemispheri- cal shells of 100 mm, 150 mm and 200 mm radius of curvature and different thicknesses are conducted to compare the shock response behaviour. It is also inferred from photographs of deformed circular plates and hemispherical shells that permanent deformation in hemi- spherical shells is very less compared to that in circular plates. The experimental peak strains are found to be in good agreement with simulation results using ANSYS Autodyn for 1.5 mm thick shell with 150 mm radius of curvature.

6.1 Scope of Future work

Present research work has been carried out with the aim to design a self acting blast closure valve to reduce the blast pressure leakage below acceptable limits. An experimental study of testing the desired blast valve with real explosive can be considered as one of the important future work. As an alternative to the experimental study with real explosive, experimental study on shock tube to impart shock loading on fully submerged blast valve can also be considered as future work. The shock structure interaction study using ANSYS Autodyn can be extended for simulation of complete hardened structure fitted with blast valves to assess the performance of blast valves. The simulation study can be extended to analyze the blast valves of bigger diameter required for large scale hardened structures.

Since the spring loaded valves are very common due to their simple and durable design, it will be important to carry out analysis of such valves for applications not only limited to Defence but also for other industries. Design modifications in the existing/ proposed valve shall also be considered for future work to make these valves available for different industrial applications. Further, the analysis of an existing blast valve developed by established companies such as Temet, Lunar etc. can be carried out using ANSYS and its performance parameters can be compared with the proposed valve design.

In addition to above, reliability and safety analysis of the blast valve can also be taken as an

important future work.

References

[1] B. A. Walton, "Designing blast hardened structures for military and civilian use," *AMPTIAC Quarterly*, vol. 6(4), 2003.

[2] P. K. Sharma, B. P. Patel, and H. Lal, "Blast valve design and related studies : A review," *Defence Science Journal*, vol. 66, No.03, pp. 242–250, 2016.

[3] E. Cohen and R. Weissman, "Blast closure systems," *In Proceedings of the sympo- sium on Protective Structures for Civilian Populations, Washington D.C.*, 1965.

[4] F. G. Ort and M. D. Mears, "Scientific director's report of atomic weapon tests at eniwetok, operation greenhouse," *Evaluation of collective-protective equipment, Maryland*, 1952.

[5] C. D. Price, "Blast closure," *US patent 3015342*, 2 January 1962.

[6] G. W. J. Ehrsam, R. Leo, and S. H. Silver, "Blast actuated closure," *US patent 3064552*, 20 November 1962.

[7] E. Cohen, "Blast valve and method of blast protection," *US patent 3075448*, 29 January 1963.

[8] R. O. Clark, "Air shock closure valve," *US patent 3115155*, 24 December 1963.

[9] J. J. Bayles and A. A. Denny, "Blast actuated closure valve and particulate filter," *US patent 3225526*, 28 December 1965. D. T. Gundersen, "Blast closure," *US patent 3278154*, 11 October 1966.

[10] O. L. Henry, "Blast closure valve," *US patent 3244194*, 05 April 1966.

[11] K. Sauter, G. Schindler, and A. Haerter, "Pressure-tight blast valve," *US patent 3489073*, 13 January 1970.

[12] J. M. Stephenson, "Blast actuated module valve," *US patent 3561346*, 09 February 1971.

[13] X. Ji, X. Lu, Y. Kang, Q. Wang, and J. Chen, "Design optimization of the bell type blast cap employed in small scale industrial circulating fluidized bed boilers," *Advanced Powder Technology*, vol. 25, pp. 281–291, 2014.

[14] TEMET, "Temet protective solutions," *Temet Oy. FI-00880 Helsinki, Finland, www.temet.com*, Accessed on 26 November 2015.

[15] "American safe room," *Oakland, http://www.americansaferoom.com*, Accessed on 26 November 2015.

[16] "Halton Marine," *http://www.halton.com*, Accessed on 26 November 2015.

[17] TEMET, "Temet combination blast valve PVE-1-150 V00032," Accessed on 26 November 2015.

[18] TEMET, "Protective solutions-Blast Valve PSV-250," *2014, www.temet.com*.

[19] TEMET, "Blast valve PSV-250," *http://www.temet.com*, Accessed on 26 November 2015.

[20] HALTON, "Blast valves," *https://www.yumpu.com/en/document/view/22150302/pv- kk-sm-smx-general-brochure-multi-column-halton*, Accessed on 26 November 2015.

[21] Halton, "PV-KK-SM and PV-KK-SMX - Blast Valves," *2014, www.halton.com*.

[22] LUNOR, "Blast valves," *http://www.lunor.ch/en/security-technology/blast-protection-valves/*, Accessed on 26 November 2015.

[23] LUNOR, "Explosion-Protection Valve - BZS T 03-007," *2014, http://www.lunor.ch/fileadmin/downloads/*.

[24] DALOC, "Components for protective installations," *www.dalocsheltec.se/en/*, Ac- cessed on 26 November 2015.

[25] ATEX, "Explosion protection," *http://www.atex100.com/*, Accessed on 26 November 2015.

[26] FIKE, "Explosion protection solutions," *http://fike.com.br/*, Accessed on 26 Novem- ber 2015.

[27] H. D. Hidallana-Gamage, D. P. Thambiratnam, and N. J. Perera, "Failure analysis of laminated glass panels subjected to blast loads," *Engineering Failure Analysis*, vol. 36, pp. 14–29, 2014.

[28] M. D. Goel, V. A. Matsagar, A. K. Gupta, and S. Marburg, "An abridged review of blast wave parameters," *Defence Science Journal*, vol. 62, No.5, pp. 300–306, 2012.

[29] R. Rajendran and J. M. Lee, "Blast loaded plates," *Marine Structures*, vol. 22, pp. 99–127, 2009.

[30] M. Larcher, G. Solomos, F. Casadei, and N. Gebbeken, "Experimental and numerical investigations of laminated glass subjected to blast loading," *International Journal of Impact Engineering*, vol. 39, pp. 42–50, 2012.

[31] K. Ramamurthy, "Explosions and explosion safety," *Tata McGraw Hill, India*, p. 288, 2011.

[32] S. E. Rigby, A. Tays, and T. Bennett, "Elastic-plastic response of plates subjected to cleared blast loads," *International Journal of Impact Engineering*, vol. 66, pp. 37–47, 2014.